AD_____

Award Number: W81XWH-10-1-0933

TITLE: Ready to Use Tissue Construct for Military Bone & Cartilage Trauma

PRINCIPAL INVESTIGATOR: Francis Y. Lee, MD, PhD

CONTRACTING ORGANIZATION: Columbia University in the City of New York
New York, NY 10032

REPORT DATE: October 2014

TYPE OF REPORT: Annual

PREPARED FOR: U.S. Army Medical Research and Materiel Command
Fort Detrick, Maryland 21702-5012

REPORT DOCUMENTATION PAGE

Form Approved
OMB No. 0704-0188

1. REPORT DATE :	2. REPORT TYPE:	3. DATES COVERED
October 2014	Annual	30 Sep 2013-29 Sep 2014

4. TITLE AND SUBTITLE
Ready to Use Tissue Construct for Military Bone & Cartilage Trauma

5a. CONTRACT NUMBER
W81XWH-10-1-0933

5b. GRANT NUMBER

5c. PROGRAM ELEMENT NUMBER

6. AUTHOR(S)
Francis Y. Lee, MD, PhD

E-Mail: fl127@columbia.edu

5d. PROJECT NUMBER

5e. TASK NUMBER

5f. WORK UNIT NUMBER

7. PERFORMING ORGANIZATION NAME(S) AND ADDRESS(ES)
Trustees of Columbia University in the City of New York
Columbia University Medical Center
650 West 168th Street, New York, NY 10032

8. PERFORMING ORGANIZATION REPORT NUMBER

9. SPONSORING / MONITORING AGENCY NAME(S) AND ADDRESS(ES)
U.S. Army Medical Research and Materiel Command
Fort Detrick, Maryland 21702-5012

10. SPONSOR/MONITOR'S ACRONYM(S)

11. SPONSOR/MONITOR'S REPORT NUMBER(S)

12. DISTRIBUTION / AVAILABILITY STATEMENT
Approved for Public Release; Distribution Unlimited

13. SUPPLEMENTARY NOTES

14. ABSTRACT

Our proposal "Ready-to-Use Tissue Construct for Military Bone and Cartilage Trauma" addresses the current limitations in treating complex, high-energy musculoskeletal wounds incurred in active combat. High-energy blast-injuries produce immediate, short-term and long-term consequences such as acute limb loss, bone loss, cartilage loss, stiffness, limping, pain, arthritis, and permanent disability, often requiring multiple reconstructive surgeries and prolonged rehabilitation. These 'osteochondral health' issues ultimately affect a soldier's quality of life both during active service and after retirement. Tissue engineering technology is a rapidly evolving field and utilizes mesenchymal cells, tissue scaffolds and growth factors. However, there are no currently available tissue-engineering constructs exhibiting 'Ready-to-Use' functionality. The most significant barrier to the practical application of tissue engineering for combat-related bone and cartilage defects is the *time- and labor-intensive process of mesenchymal stem cell expansion*. The **goal** of this proposal is to introduce a new tissue engineering paradigm to the Defense Health Program (**DHP**) by utilizing a biomechanically competent and anatomically matched tissue construct without resorting to the cumbersome process of mesenchymal stem cell expansion.

15. SUBJECT TERMS
Ready to use tissue construct, biomechanically competent anatomically matched tissue construct

16. SECURITY CLASSIFICATION OF:			17. LIMITATION OF ABSTRACT	18. NUMBER OF PAGES	19a. NAME OF RESPONSIBLE PERSON
					USAMRMC
a. REPORT	b. ABSTRACT	c. THIS PAGE			19b. TELEPHONE NUMBER *(include area code)*
U	U	U	UU	38	

Table of Contents

1. INTRODUCTION (excerpted from grant)

Our study "Ready-to-Use Tissue Construct for Military Bone and Cartilage Trauma" addresses current limitations in treating complex, high-energy musculoskeletal wounds incurred in active combat. High-energy blast-injuries produce immediate, short-term and long-term consequences such as acute limb loss, bone loss, cartilage loss, stiffness, limping, pain, arthritis, and permanent disability, often requiring multiple reconstructive surgeries and prolonged rehabilitation. These 'osteochondral health' issues ultimately affect a soldier's quality of life both during active service and after retirement. Tissue engineering technology is a rapidly evolving field and utilizes mesenchymal cells, tissue scaffolds and growth factors. However, there are no currently available tissue-engineering constructs exhibiting 'Ready-to-Use' functionality. The most significant barrier to the practical application of tissue engineering for combat-related bone and cartilage defects is the *time- and labor-intensive process of mesenchymal stem cell expansion*. The goal of the current study is to introduce a new tissue engineering paradigm to the Defense Health Program (DHP) by utilizing a biomechanically competent and anatomically matched tissue construct without resorting to the cumbersome process of mesenchymal stem cell expansion. Our project utilizes a series of *in vivo* large animal translational experiments that will hopefully lead to the development of new military technology products and utilities for the definitive and preventive orthopaedic care of military personnel and retirees. The project has 3 major aims, excerpted from the revised Statement of Work and listed below:

Aim 1. To examine whether our prefabricated constructs can reconstitute osteochondral defects of critical-size in a canine distal femoral condyle defect model simulating high-energy blast-injury. Osteochondral injuries of any size require anatomically perfect reconstruction to prevent pain and post-traumatic arthritis. We hypothesize that anatomically-conforming osteochondral constructs with controlled release of TGF-β3 can reconstitute physiologic *hyaline cartilage*-osseous transition in massive osteochondral defects in large animals. We will conduct functional outcome analysis, X-ray/MRI examination and histologic analysis.

Aim 2. To examine whether our prefabricated construct can reconstitute critical size segmental defects in canine tibiae. Critical-size segmental defects in long bone diaphyses require extensive reconstructive procedures and prolonged rehabilitation times. We hypothesize that our *Ready-to-Use* constructs can successfully restore 3 cm critical size segmental defects in dog tibiae. We will examine the incorporation and regeneration of the biogenic implant with host bone by conducting functional outcome assessments, radiography, biomechanical torsional testing and histologic examination.

Aim 3. To examine biomechanical suitability of ready-to-use constructs in massive osteochondral defects and segmental bone defects in human cadaveric femora. We have successfully developed anatomically conforming bone and cartilage constructs for rats and rabbits. Early joint motion and ambulation are important in human patients. We hypothesize that our *ready-to-use* construct can maintain the biomechanical and functional properties in human cadaveric bones under simulated physiologic load. We intend to optimize and adapt our "ready-to-use" scaffold construct for humans. We will verify the biomechanical competence in a critical size defect in human femora and knee joints by simulating loads seen during ambulation and knee range of motion.

Our central hypothesis is that an anatomically and biomechanically compatible scaffold with TGF-β3 and BMP-2 can reconstitute massive cartilage/bone defects without exogenous MSCs. The goal of this Technology Development Project is to simplify the current paradigm of tissue engineering by 1) eliminating the need for time- and labor-intensive stem cell harvesting and expansion and 2) adopting anatomically conforming constructs which promote incorporation, remodeling, early joint motion, partial weight bearing, and ambulation. Our hypothesis is based on compelling preliminary data in small animal models, such as mice, rats and rabbits. The current protocol will take another step towards military application by verifying successful regeneration of cartilage (**Aim 1)** and bone (**Aim 2**) in massive canine bone defects and by confirming biomechanical and functional suitability in human cadaveric knee and tibia defect models (**Aim 3**). **Aim 1** and **Aim 2** are significant in that they will introduce a simpler, more cost-effective approach to tissue engineering that obviates the need for extensive cell culturing and laboratory support. **Aim 3** is significant in that the injured soldiers can start early rehabilitation and ambulation following reconstructive surgeries using Ready-to-Use anatomically and biomechanically conforming biogenic scaffolds.

2. BODY

2.0 Overview

We followed our current Columbia and USAMRMC Animal Care and Use Review Office (ACURO) approved IACUC protocol and performed surgeries on eleven additional Aim 2 (segmental defects) dogs for the period November 2013 through October 2014. All segmental defect dogs received scaffolds composed of 90% poly-caprolactone (PCL) and 10% hydroxyapatite (HA) by weight (PCL+HA). Five dogs received unseeded scaffolds, three dogs received scaffolds seeded with BMP-2, and the remaining three dogs received canine cadaveric allografts. Three segmental defect dogs had received scaffolds seeded with BMP-2 in September 2013 completed their recovery phase during reporting period. In summary, fourteen segmental defect dogs were successfully taken to the full 16 week duration of the experiment and then humanely sacrificed. The purpose of these surgeries was threefold, a) to demonstrate that the surgery did not result in excessive pain and discomfort to the animal; b) to demonstrate that there was no immune response to the implanted scaffolds; and c) to demonstrate the stable performance and outcome of this technique.

Immediately after euthanizing, both hind tibias were dissected and harvested with soft tissue, and were stored at -80 deg C for later mechanical testing. Mechanical testing was not performed on any of these tibiae because the testing equipment was not available due to the renovation of our laboratory space. All the stored tibiae will undergo mechanical testing upon completion of renovation in the early spring of 2015.

As per protocol, radiographs were taken on a bi-weekly basis for all segmental defect dogs to document the progression of bony healing. Outcome measures were recorded throughout the 16 week experimental period for all dogs. Hard section histology was completed for two segmental defect dogs (one unseeded scaffold, one canine allograft) for which the results were reported in 2012 annual report.

The subsections to follow will elaborate on the above accomplishments and experimental results.

2.1 Aim 1 - Osteochondral Defects

No osteochondral defect surgeries were performed during this reporting period because of a significant reduction in the amount of available cage space due a major renovation of Columbia University's animal facilities. It was decided to use the cage space that was available for segmental defect surgeries (Aim 2) so that a sufficient number of dogs could be completed to provide a large enough n for meaningful analyses.

2.2 Aim 2 - Segmental Defects

Radiologic images of the hind limbs following surgery were obtained for all segmental defect dogs. Outcome measures were also recorded on a nominally daily basis throughout the 16 week recovery period. Details are provided below.

2.2.1 Segmental Defect Scaffold Manufacturing

The objective of the segmental defect scaffold is to promote bony ingrowth into the subchondral bone. The segmental defect scaffold architecture is based on the work of Lee et al, (Lancet 2010) (1) one of the researchers on this grant. The scaffold has no outer cortex layer and an 8 mm lumen to permit the infusion of bone marrow material through the lumen and into the scaffold through the surface pores. The scaffolds were made 20 mm long to represent a critical size defect in the dog (1). A new 3-D printer type (3D-Bioplotter, EnvisionTec, Germany) was obtained in April 2014 with better resolution than the Bioplotter used to create the previous scaffolds. Slight changes to the control parameters were optimized for the new device, as well as a minor change to a molecular weight (MW) of 45,000 for the raw PCL material (Polycarprolacton, SigmaAldrich Co. USA). The working temperature of the new 3-D printer was optimized to 103 deg Celsius. Other conditions were kept same as for the previous two years.

2.2.2 Segmental Defect Surgeries

Segmental defect surgeries were done in accordance to the approved IACUC protocol as detailed in the 2013 Annual Report. The broad 3.5-mm-8-hole locking compression plate (LCP) system from the Synthes® veterinary division (West Chester, PA) was used for all 11 dogs operated on during this reporting period and for the 3 dogs from the previous reporting period that were sacrificed during this reporting period. None of the dogs experienced any untoward events. A very slight amount of plate bending in one of the dogs was observed, but this very slight bend did not demonstrate any significant clinical manifestations and did not progress with time. Therefore, it was concluded that the use of broad LCP was a significant improvement to the standard plate and will be used in all subsequent surgeries.

2.2.3 Segmental Defect Radiographs

Digital radiographs were taken of all segmental defect dogs every two to four weeks. The dogs with BMP-2 scaffolds (segmental defect dog 8, 9, 10 12, 13 and 14) qualitatively demonstrated more callus formation than the dogs with unseeded scaffolds (segmental defect dog 11, 15, 18, 19 and 21) four weeks post-surgery. The dogs implanted with the scaffolds made by the new 3-D printer (dog 18, 19 and 21) demonstrated the same healing process compared with the Bioplotter scaffolds.

As mentioned above the broad LCP successfully prevented plate bending from occurring. Slight bending was observed for Dog 15, possibly because of less than optimal scaffold placement during surgery. The bending first appeared at four weeks Figure 8 and did not progress the remaining twelve weeks to sacrifice.

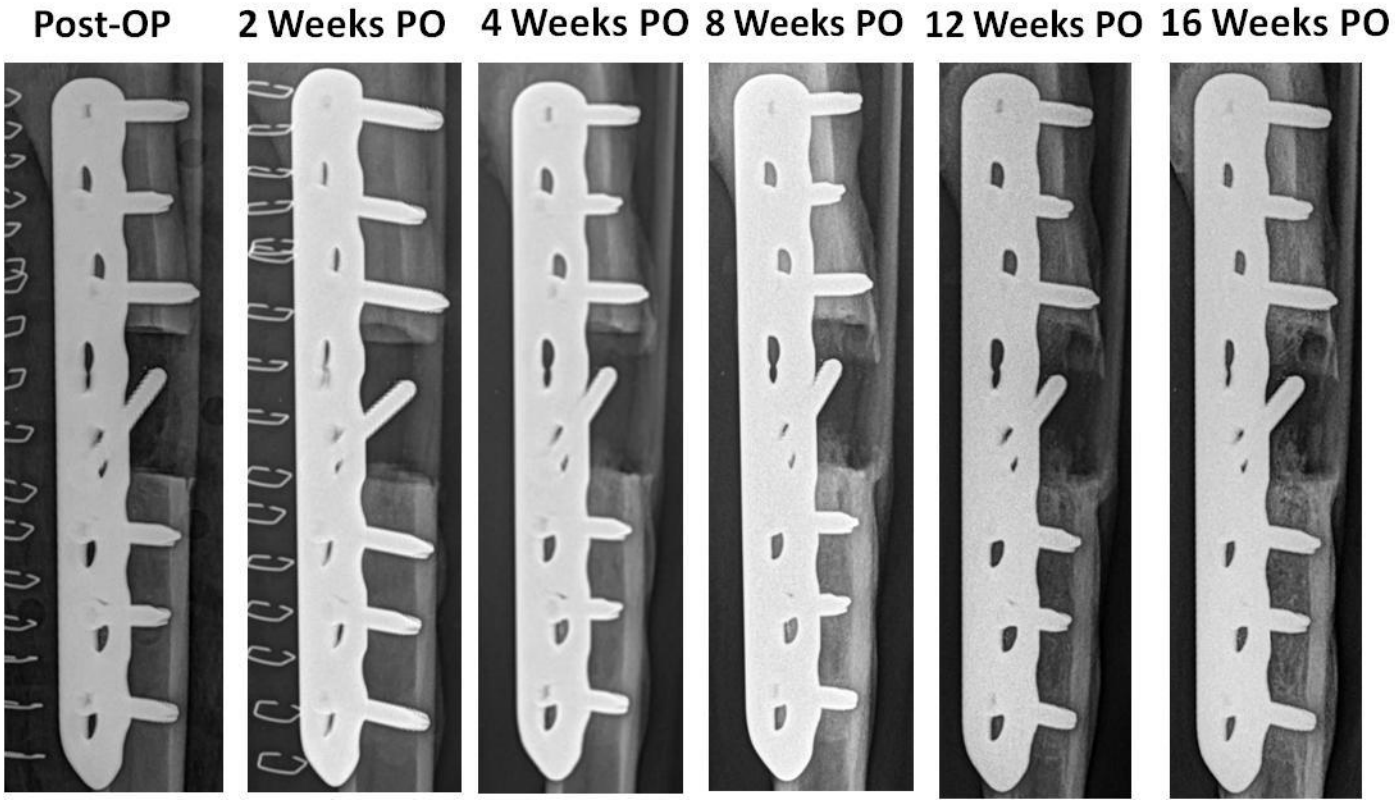

Figure 1: Radiographs of lateral view for Segmental Defect Dog 8 (BMP-seeded scaffold) as a function of time showing.

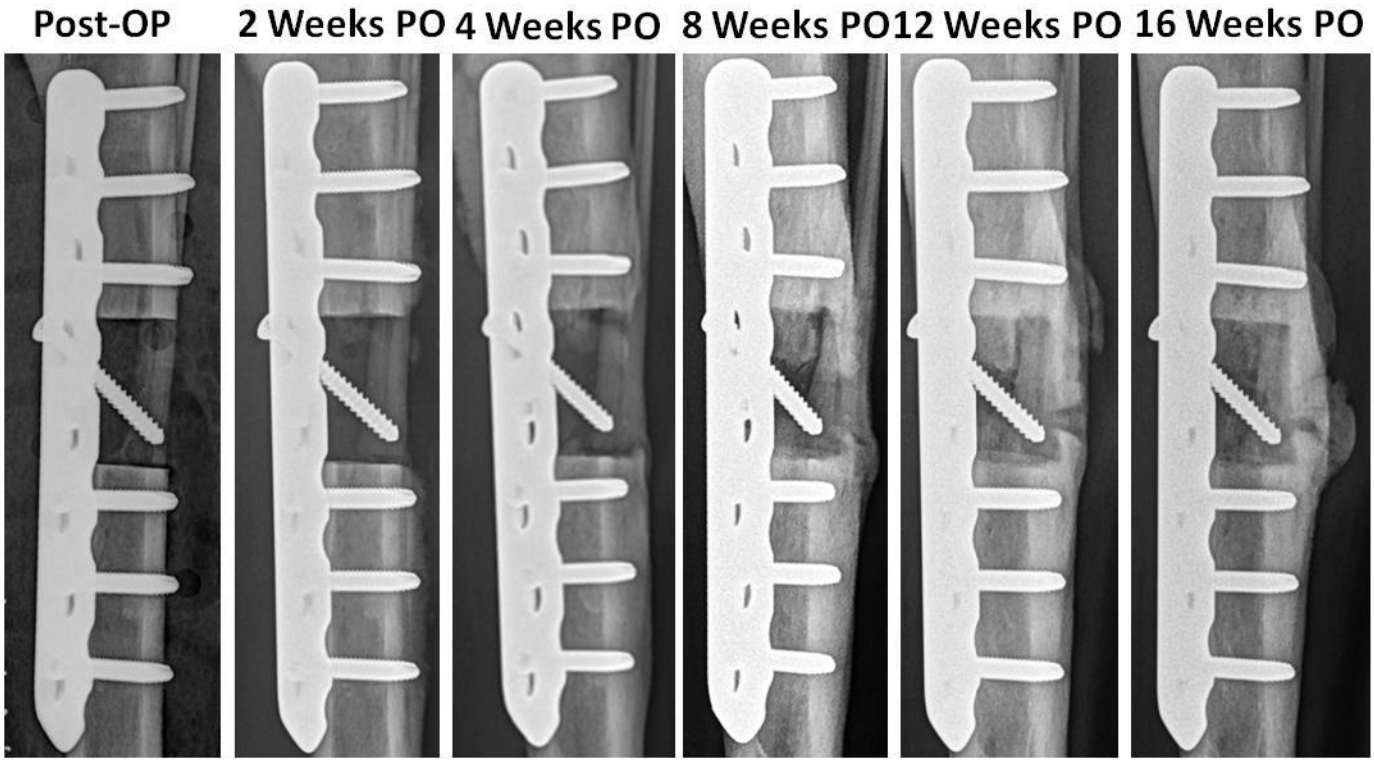

Figure 2: Radiographs of lateral view for Segmental Defect Dog 9 (BMP-seeded scaffold) as a function of time showing.

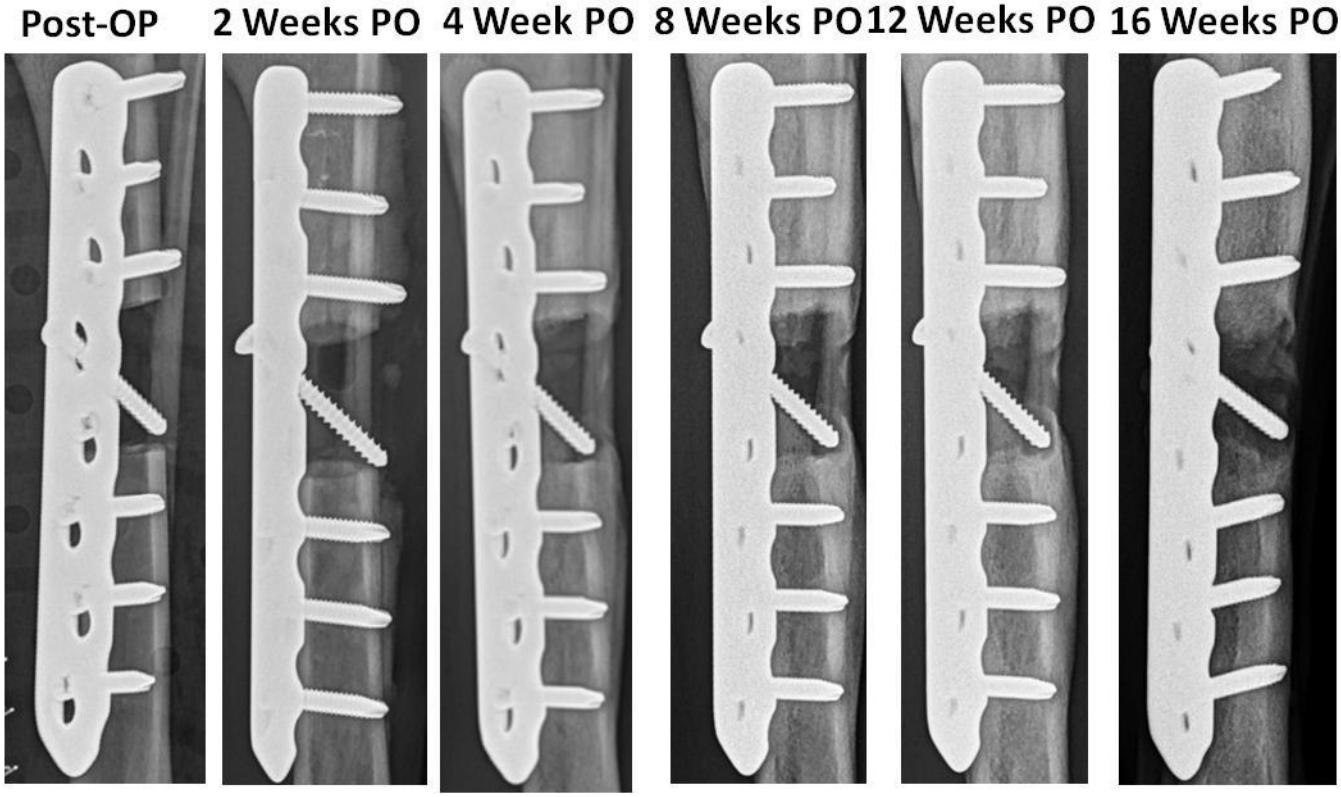

Figure 3: Radiographs of lateral view for Segmental Defect Dog 10 (BMP-seeded scaffold) as a function of time showing.

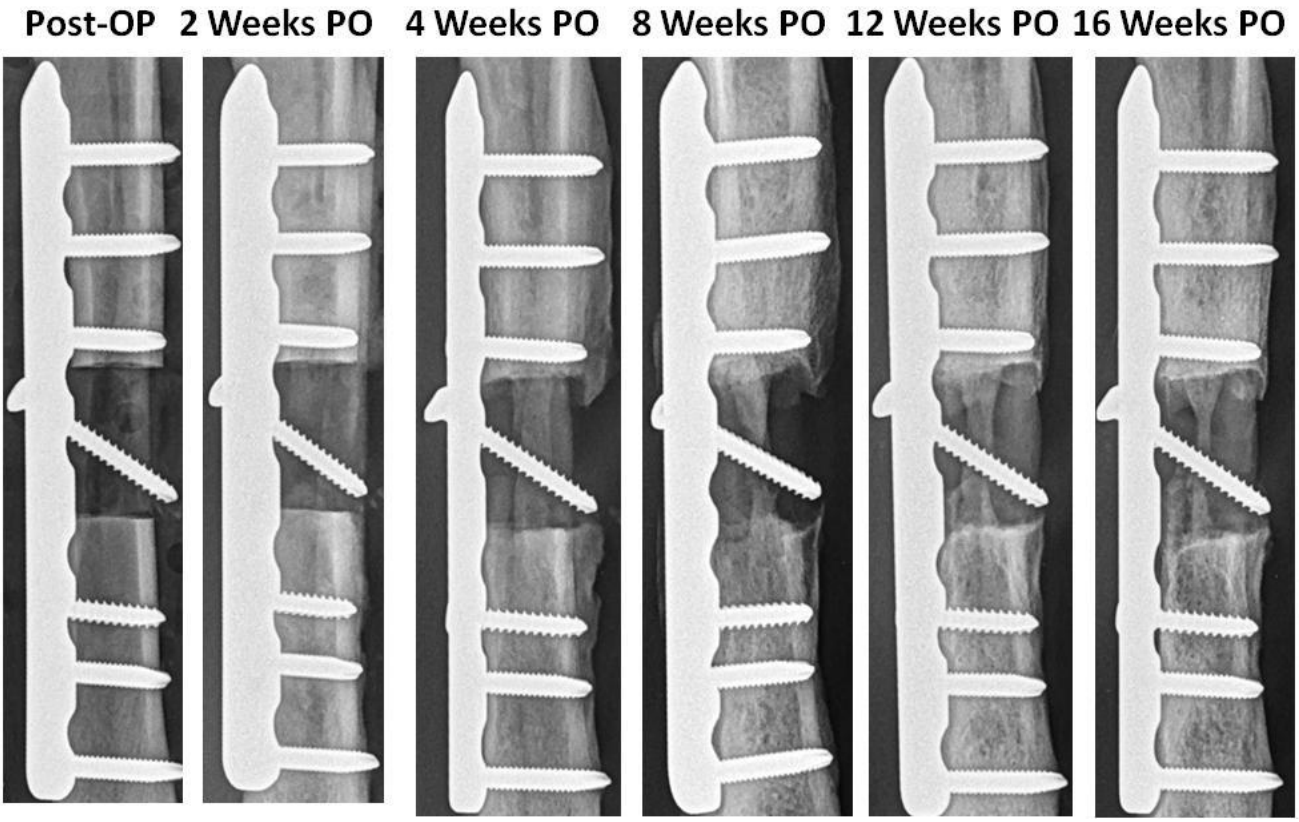

Figure 4: Radiographs of lateral view for Segmental Defect Dog 11 (unseeded scaffold) as a function of time showing.

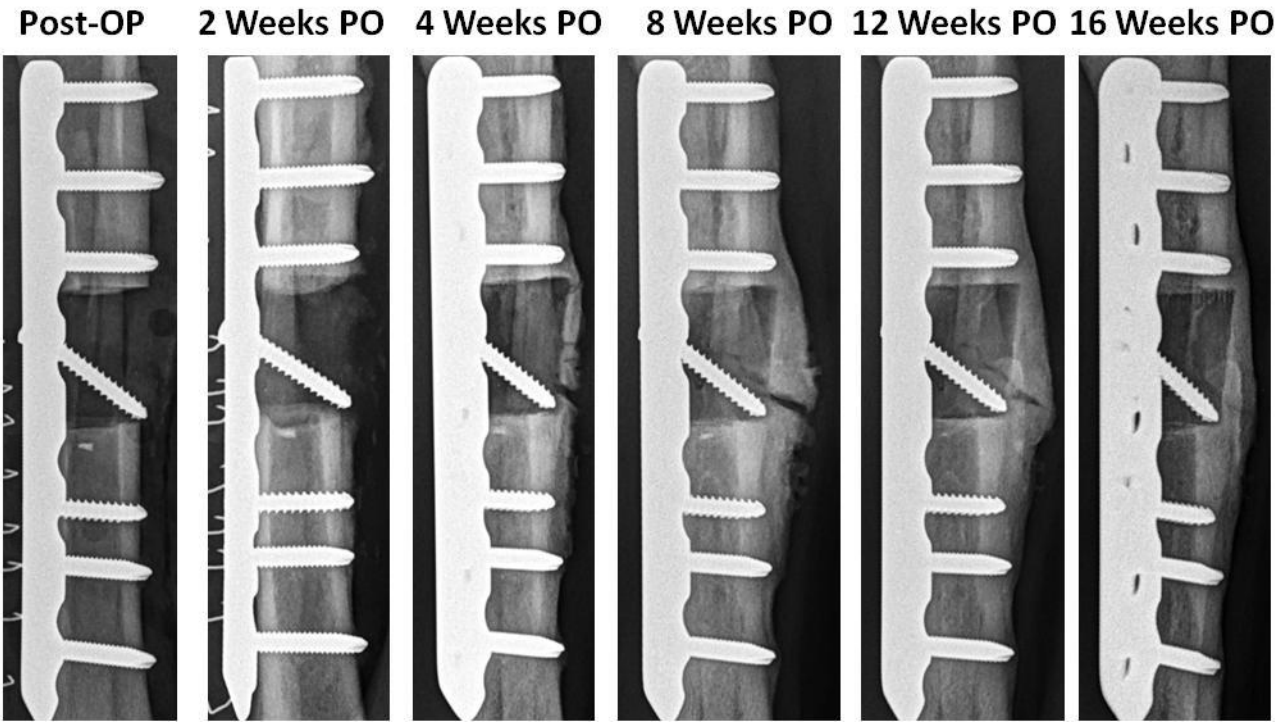

Figure 5: Radiographs of lateral view for Segmental Defect Dog 12 (BMP-seeded scaffold) as a function of time showing.

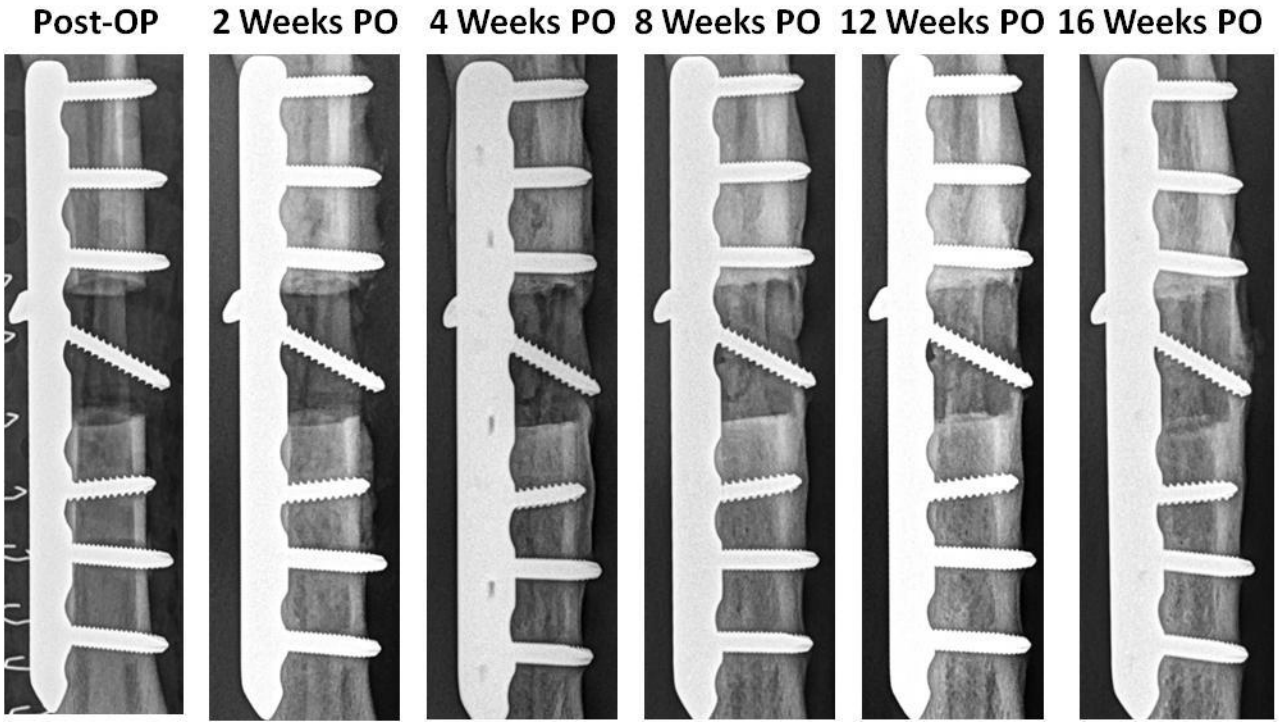

Figure 6: Radiographs of lateral view for Segmental Defect Dog 13 (BMP-seeded scaffold) as a function of time showing.

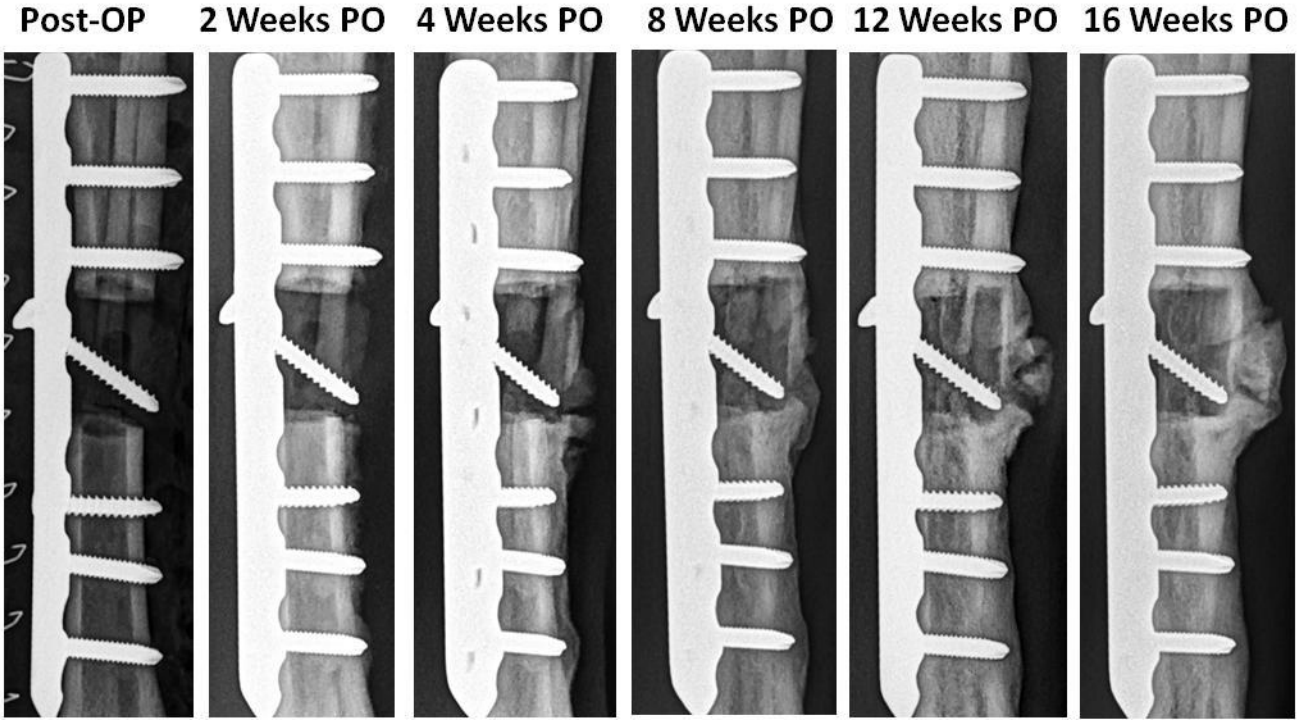

Figure 7: Radiographs of lateral view for Segmental Defect Dog 14 (BMP-seeded scaffold) as a function of time showing.

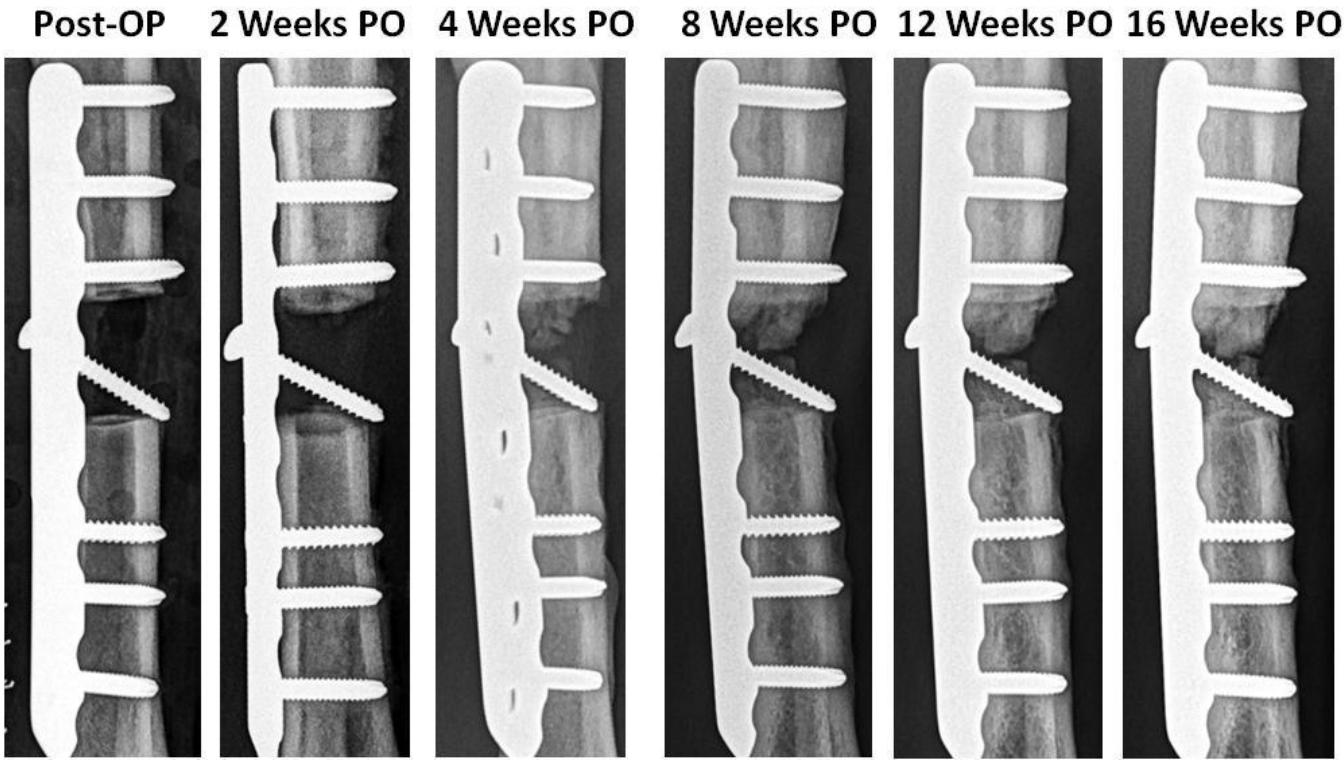

Figure 8: Radiographs of lateral view for Segmental Defect Dog 15 (unseeded scaffold) as a function of time showing.

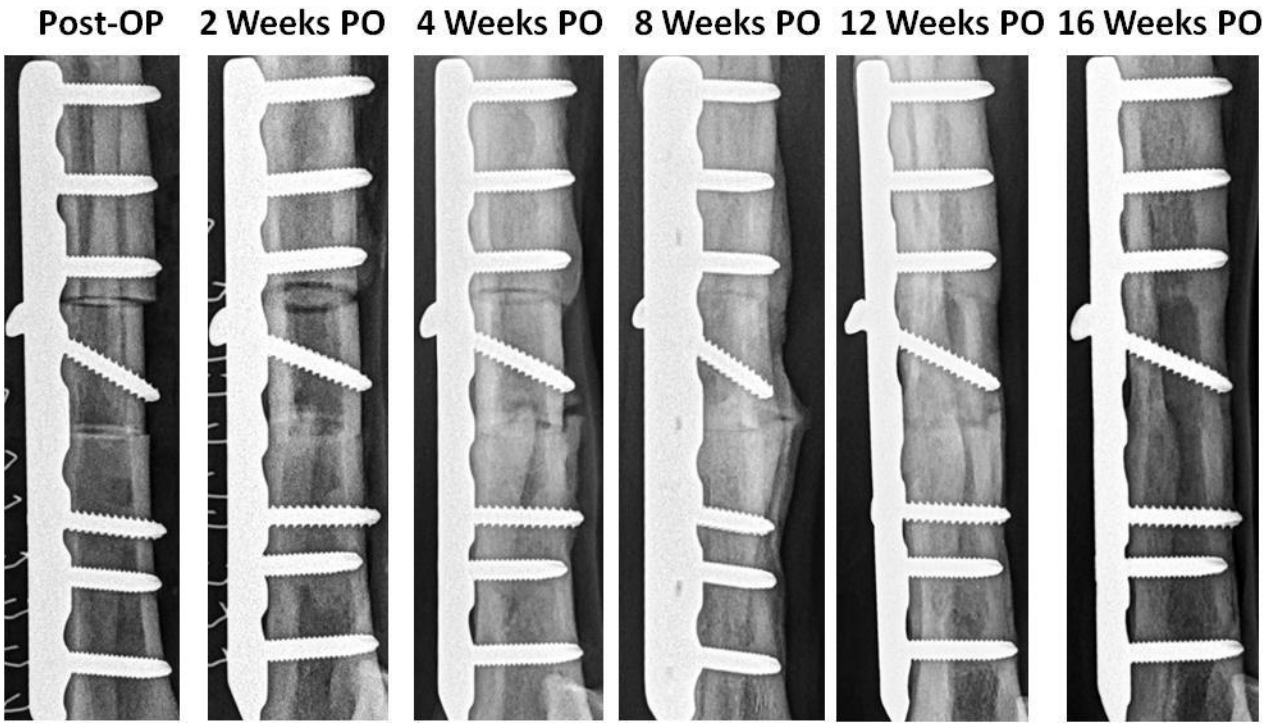

Figure 9: Radiographs of lateral view for Segmental Defect Dog 16 (allograft) as a function of time showing.

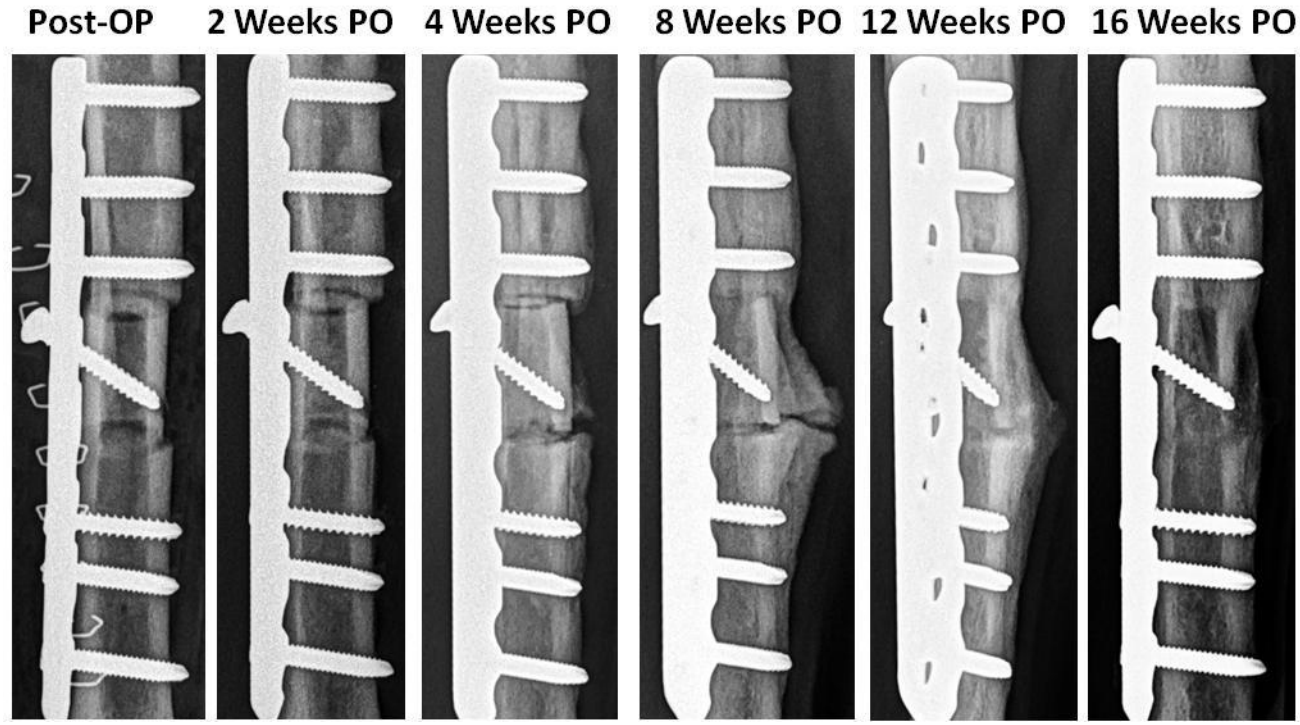

Figure 10: Radiographs of lateral view for Segmental Defect Dog 17 (allograft) as a function of time showing.

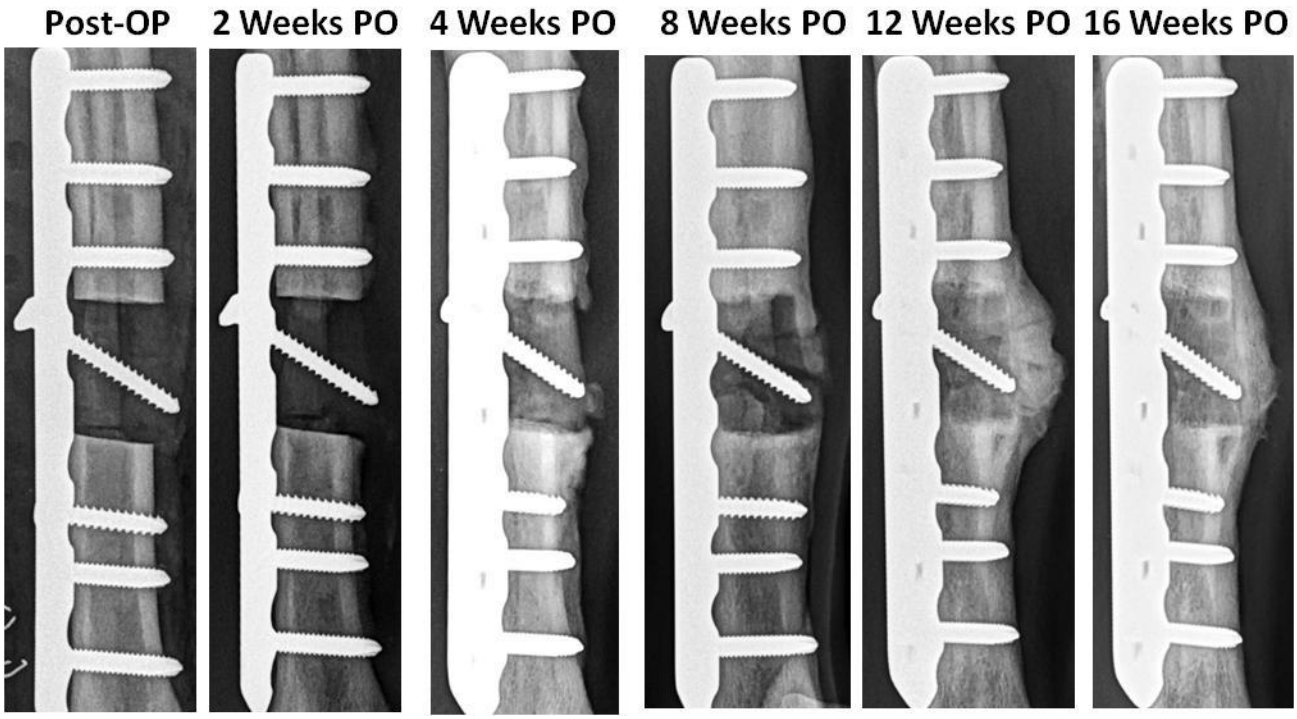

Figure 11: Radiographs of lateral view for Segmental Defect Dog 18 (unseeded scaffold) as a function of time showing.

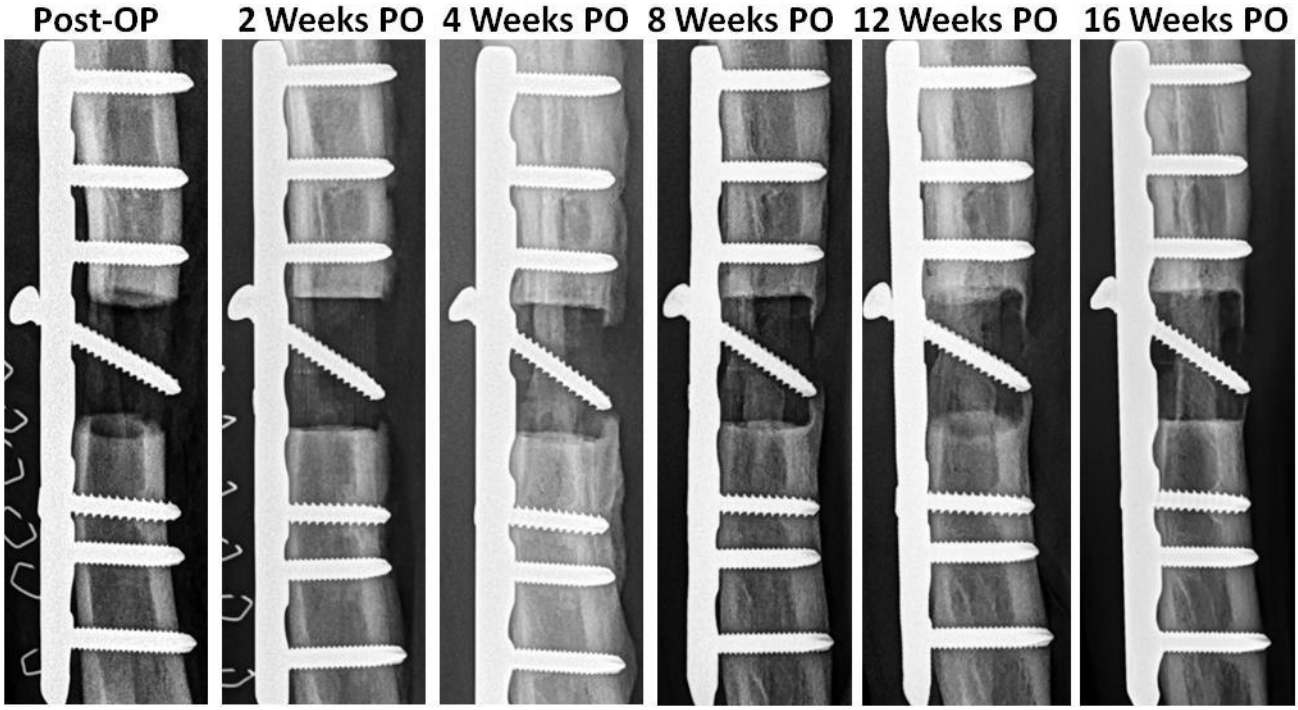

Figure 12: Radiographs of lateral view for Segmental Defect Dog 19 (unseeded scaffold) as a function of time showing.

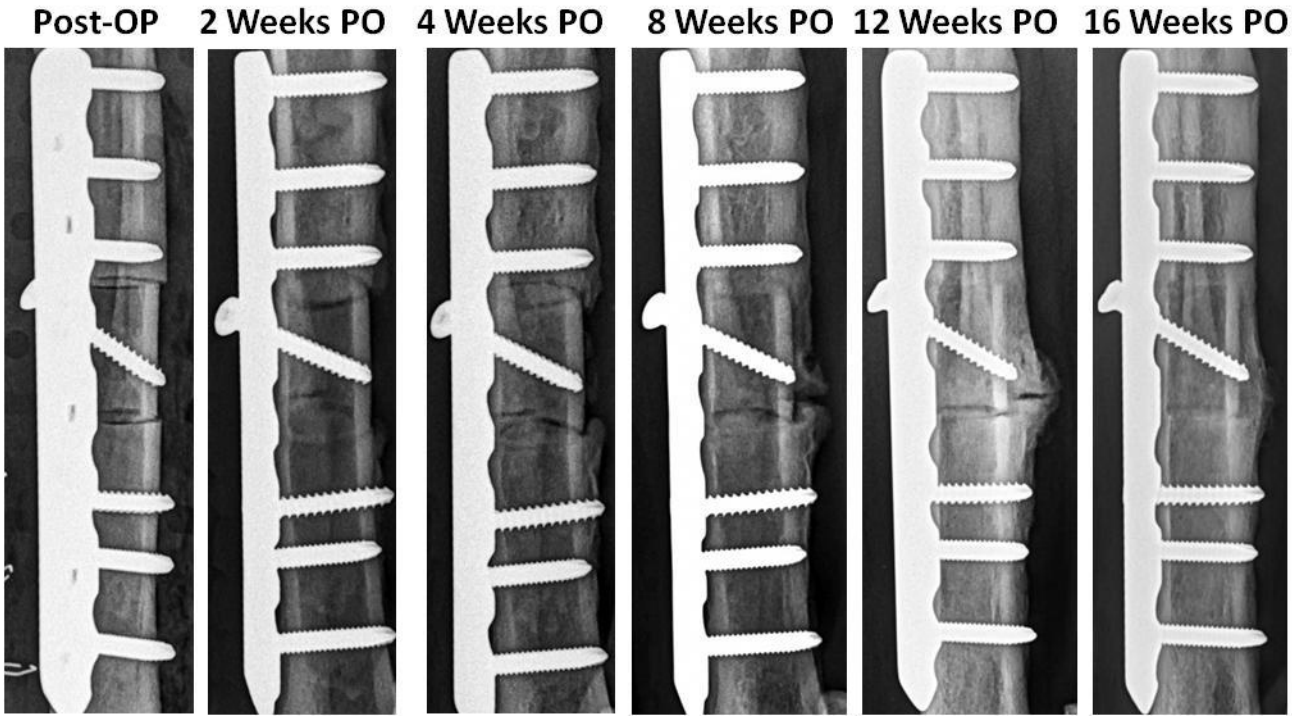

Figure 13: Radiographs of lateral view for Segmental Defect Dog 20 (allograft) as a function of time showing.

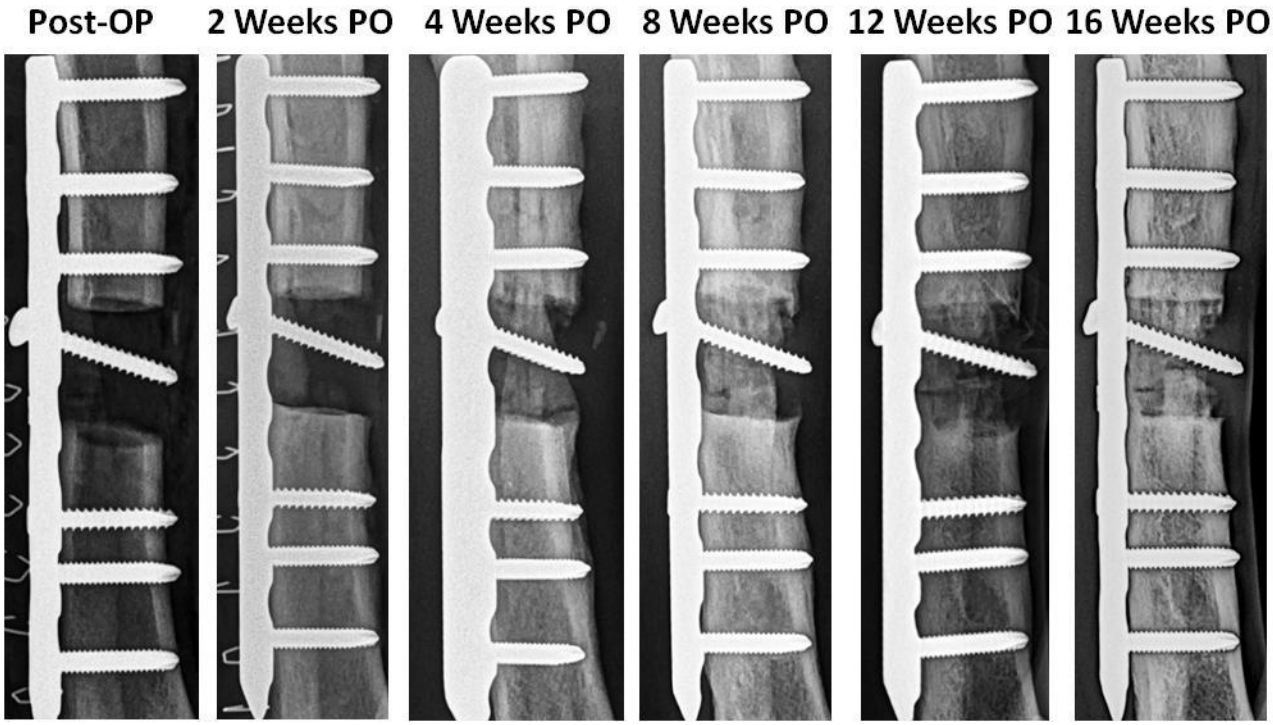

Figure 14: Radiographs of lateral view for Segmental Defect Dog 21 (unseeded scaffold) as a function of time showing.

2.2.4 Segmental Defect Outcome Measures

Outcome measures of gait, lameness, pain, knee motion and an aggregate of these measures were nominally recorded for each dog every weekday (refer to Table 1 for criteria), excluding Saturdays and Sundays. Using the 19 successful segmental defect dogs completed to date, three experimental arms of Aim 2 were compared using a generalized linear model two-way ANOVA (SAS, Cary, N.C.). Treatment (unseeded scaffolds, BMP-2 scaffolds and allografts) was an unrepeated factor and time point (14 days, 28 days, 56 days, 84 days and 112 days) was a repeated factor. A Student-Newman Keuls multiple comparisons test was used to discern differences between levels. Statistical significance was taken as $p < 0.05$. The BMP-2 group demonstrated a qualitatively better healing and higher outcome scores ($p < 0.0001$) than either the unseeded scaffolds or the allograft groups. Figure 16, 17 and 19 showed the total scores of those dogs entering the "good" range (6~7 scores) at the twentieth day post-surgery. Figures 15, 20 and 21 show an earlier good score at approximately two weeks. The effect of time point was also found to be highly significant ($p < 0.0001$), with a monotonic improvement with time. The lowest scores were for 14 days and were statistically lower than the 28 day and 56 day time points. The 112 day time point had the highest total score. The good scores at day twenty can also be seen in the corresponding radiographs: more bony growth and coverage of the scaffold corresponding to less pain and discomfort in the dogs. The six dogs in the BMP-2 group qualitatively showed faster healing than the two groups and the scores of the BMP-2 group in the late period close to sacrifice had higher values than the other two groups. The allograft group (Figure 23, 24, 27) also entered the good range at around the twenty-second day, which was earlier than the dogs in the unseeded group. Segmental Defect Dog 15 had a slight amount of plate bending that seemed to delay its bone healing and may have made it more uncomfortable as demonstrated by fluctuation of the scores between seventy and eighty days, however the overall scores of this dog remained in the good range.

Outcome	Criteria	Range
Gait	Non weight-bearing	0
	Partial weight-bearing	1
	Full weight-bearing	2
Lameness	Does not use limb during walking	0
	Partial use of affected limb, walks with noticeable limb	1
	No lameness when walking	2
Pain	Severe reaction to touch, withdraws upon the slightest touch with guarding behavior and/or vocalization	0
	Mild reaction to touch, withdraws limb upon touch	1
	No reaction to touch of affected limb	2
Knee Motion	Significant reduction in range of motion (0-30%)	0
	Moderate reduction in range of motion (30-60%)	1
	Slightly reduced range of motion (60-80 %)	2
	Normal range of motion (90-100%, preoperative range)	3
Total		0-9

Table 1: Criteria used to grade Outcome Measures for Segmental Defect Dogs.

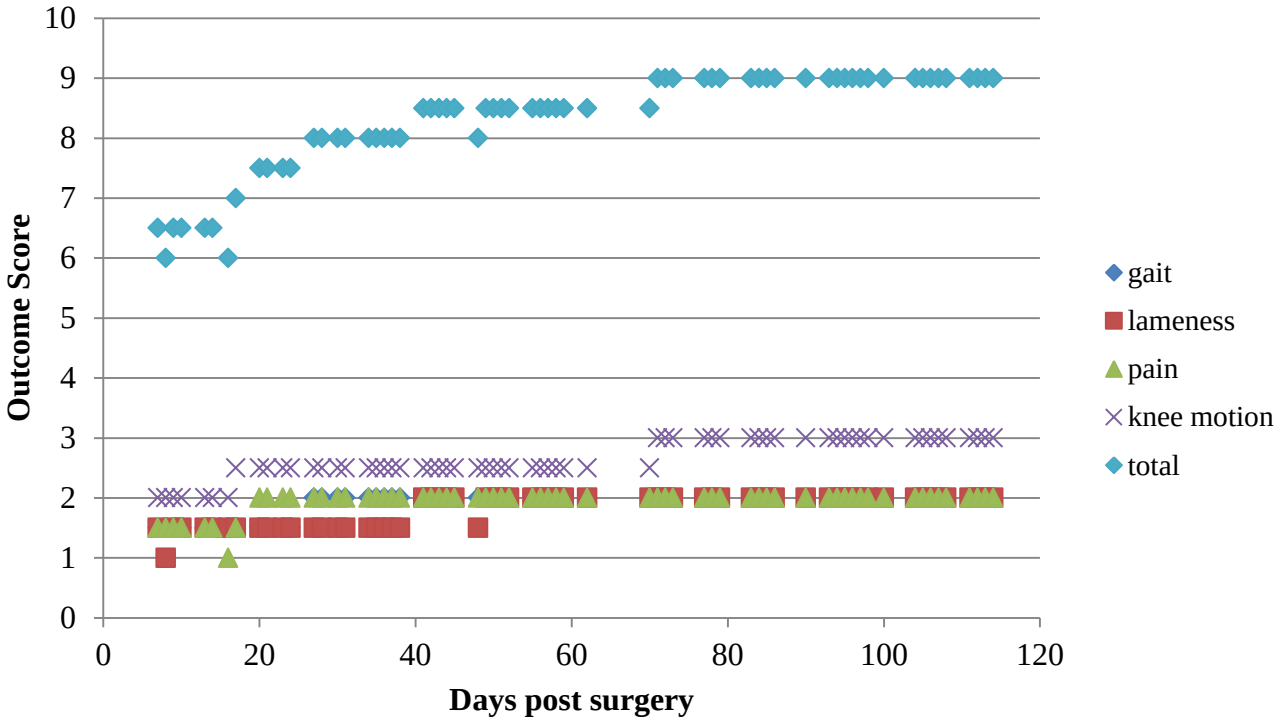

Figure 15: Outcome measurement for Segmental Defect Dog 8 (BMP-seeded scaffold).

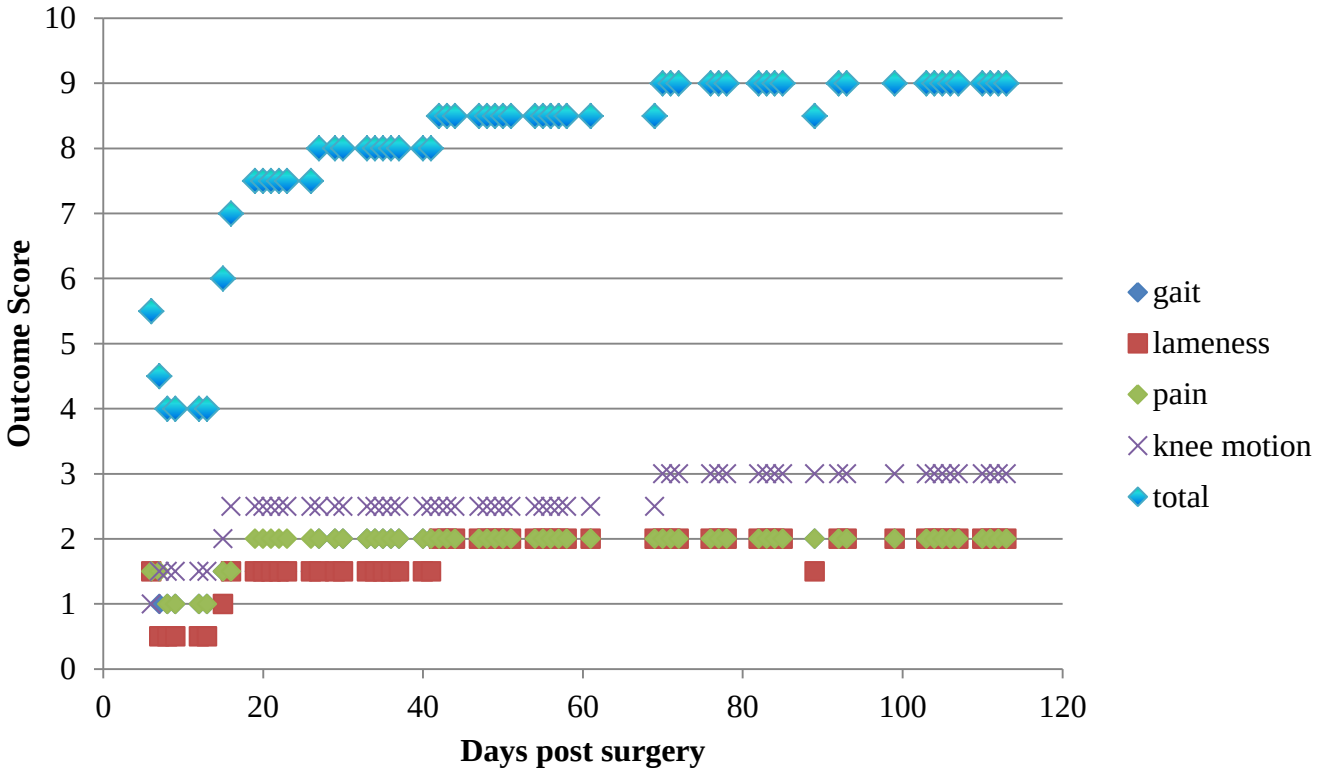

.
Figure 16: Outcome measurement for Segmental Defect Dog 9 (BMP-seeded scaffold).

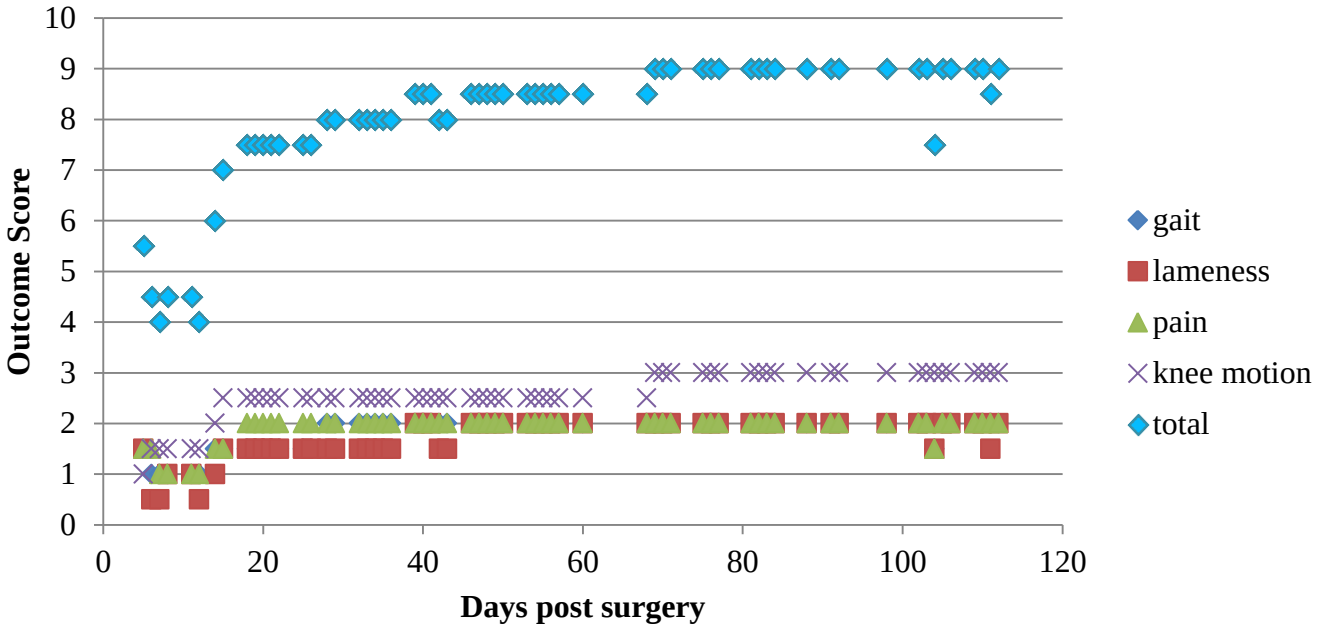

Figure 17: Outcome measurement for Segmental Defect Dog 10 (BMP-seeded scaffold).

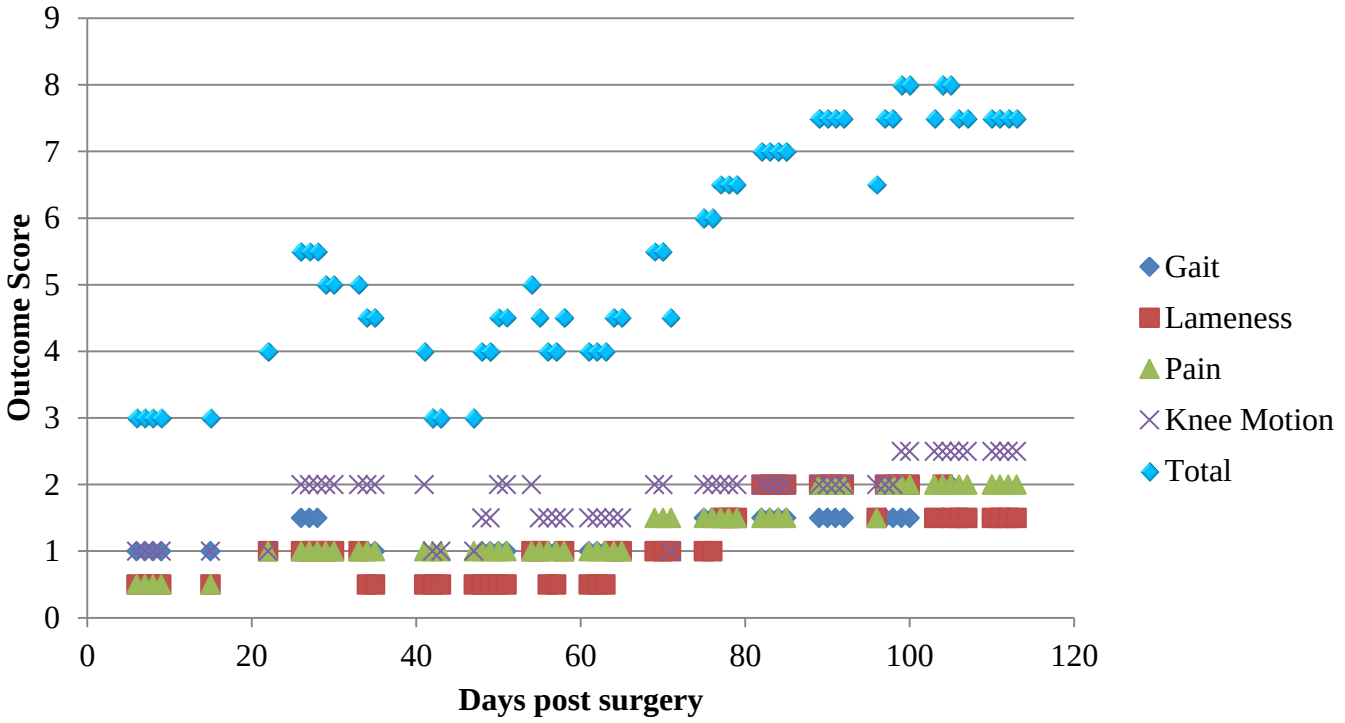

Figure 18: Outcome measurement for Segmental Defect Dog 11 (unseeded scaffold).

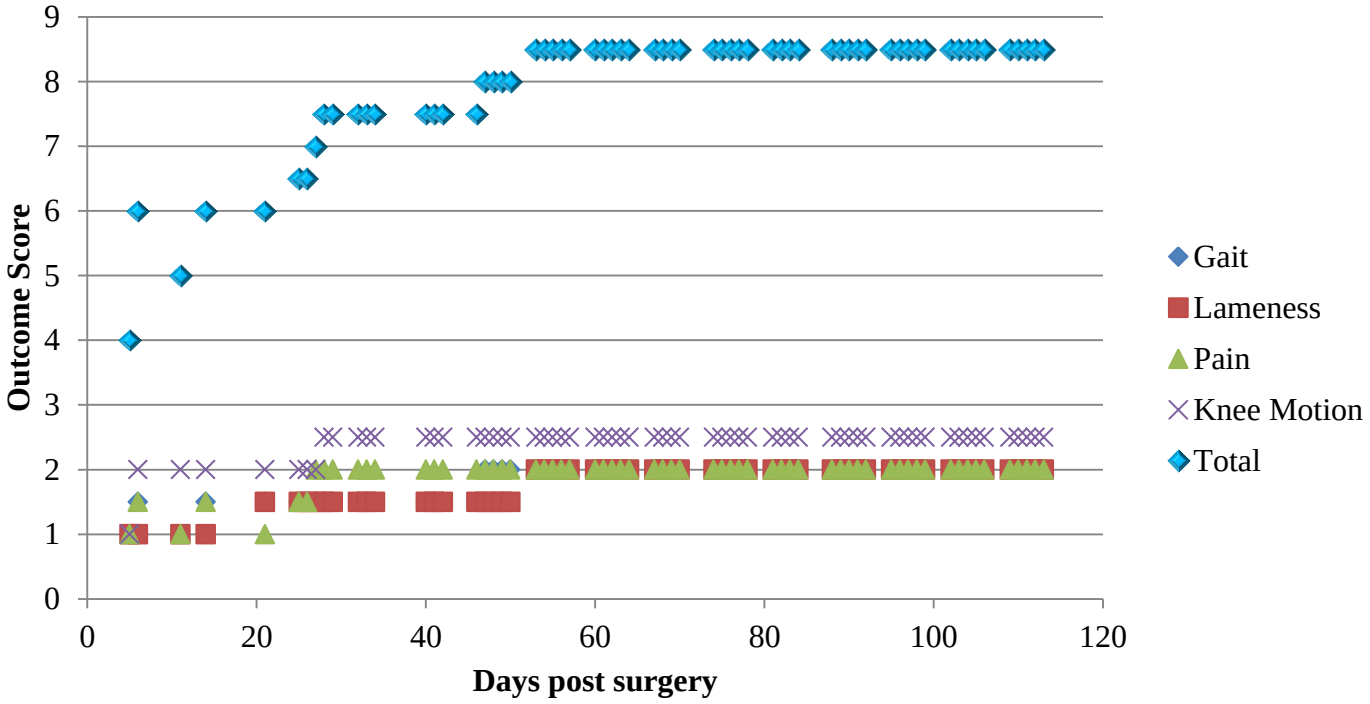

Figure 19: Outcome measurement for Segmental Defect Dog 12 (BMP-seeded scaffold).

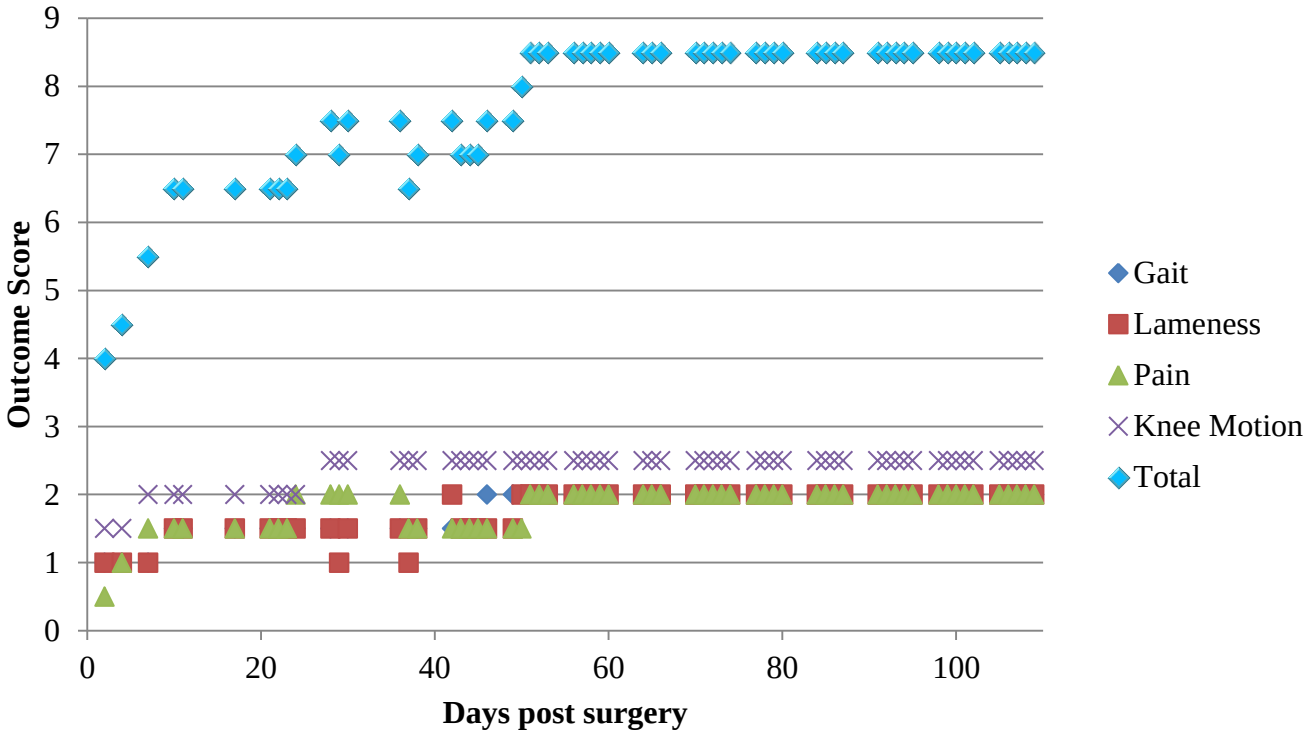

Figure 20: Outcome measurement for Segmental Defect Dog 13 (BMP-seeded scaffold).

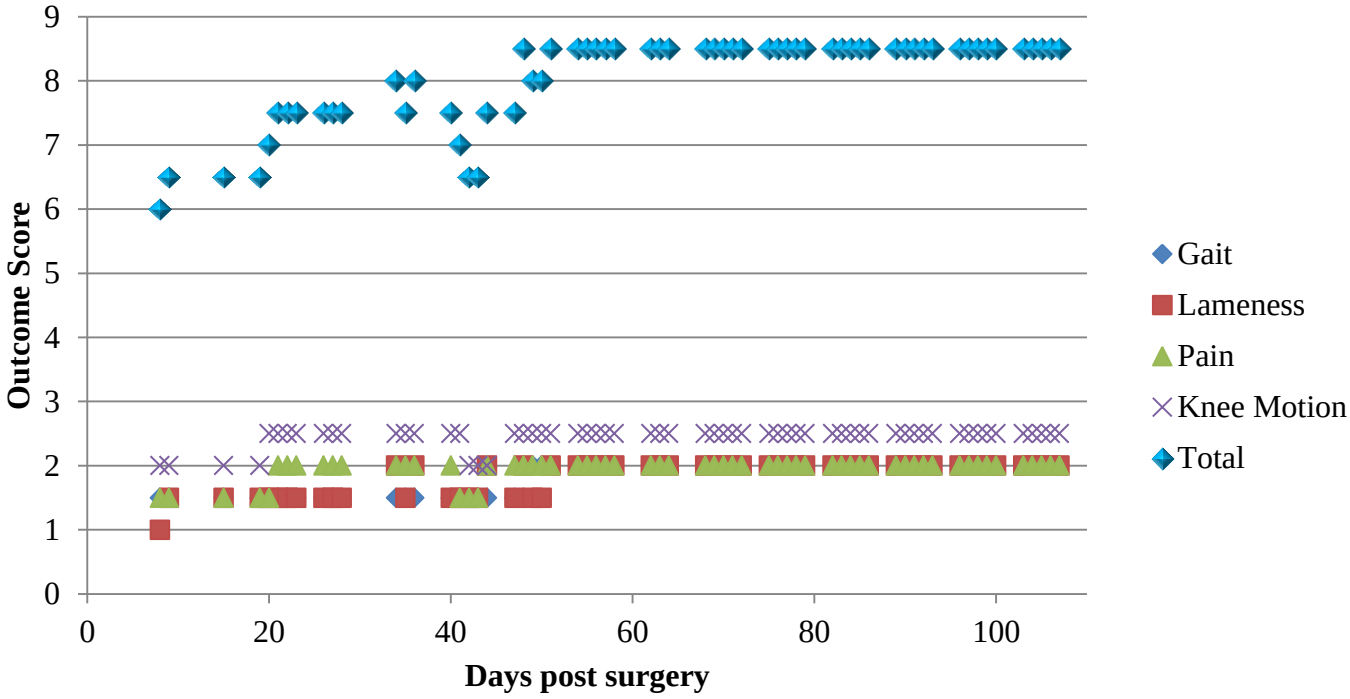

Figure 21: Outcome measurement for Segmental Defect Dog 14 (BMP-seeded scaffold).

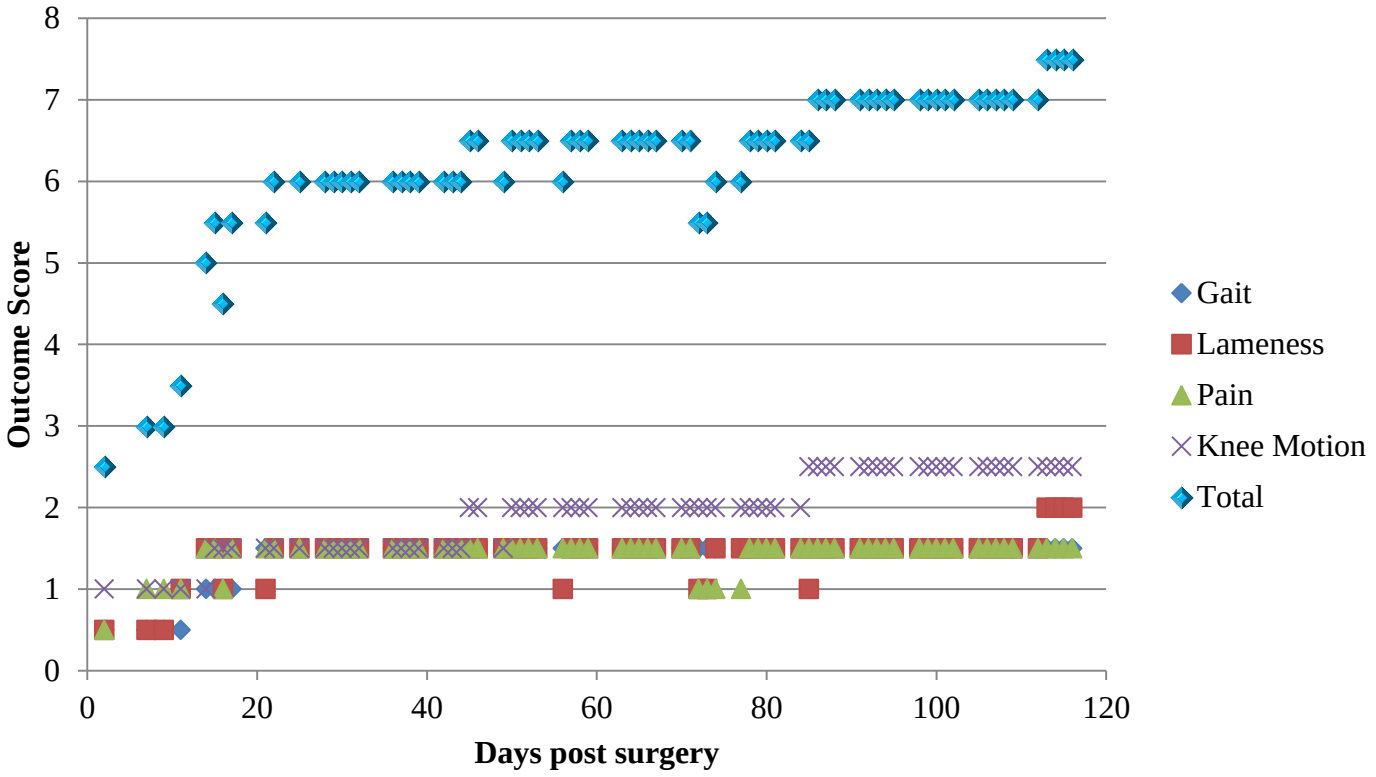

Figure 22: Outcome measurement for Segmental Defect Dog 15 (unseeded scaffold).

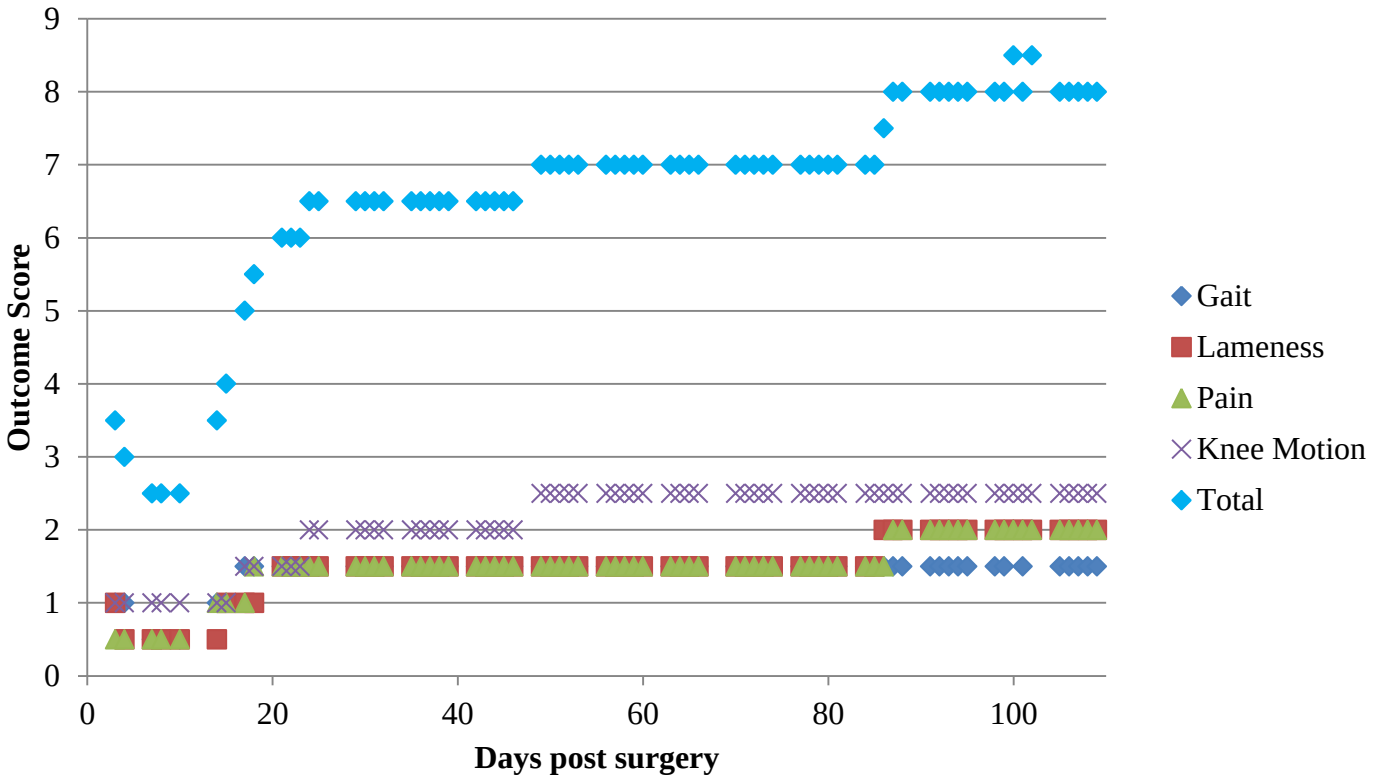

Figure 23: Outcome measurement for Segmental Defect Dog 16 (allograft).

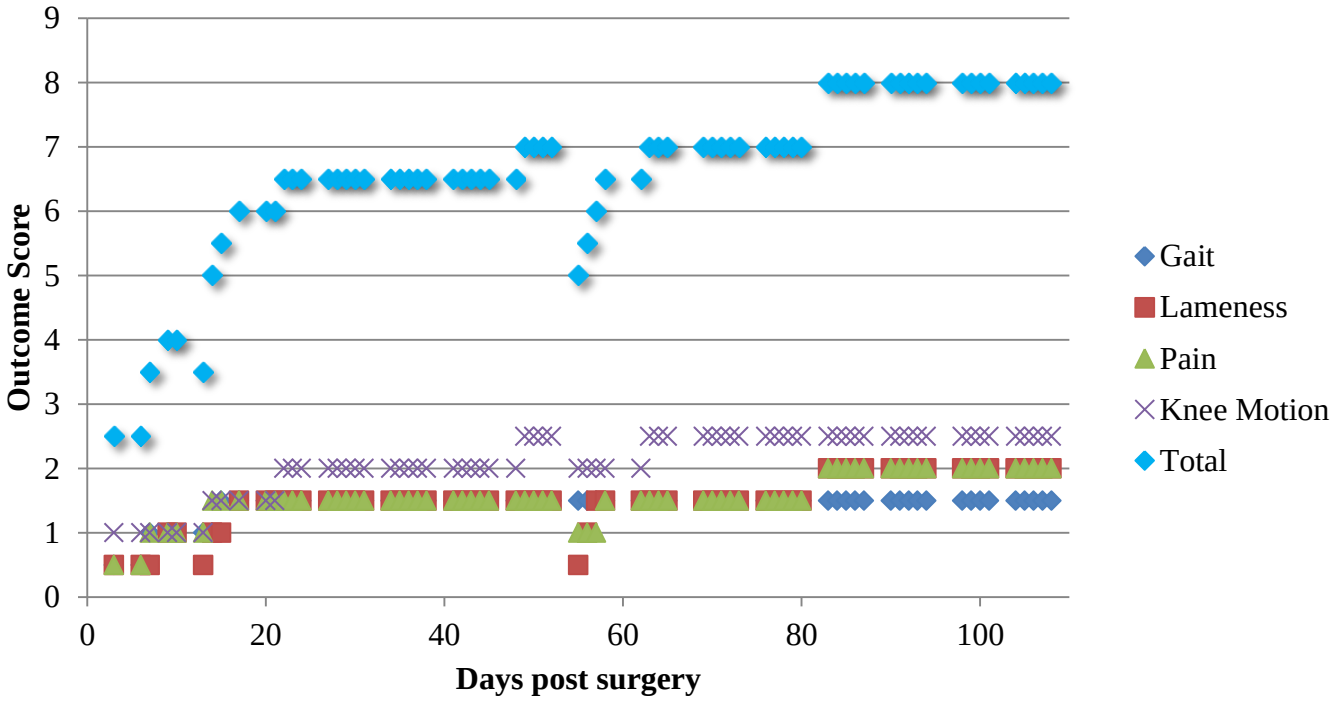

Figure 24: Outcome measurement for Segmental Defect Dog 17 (allograft).

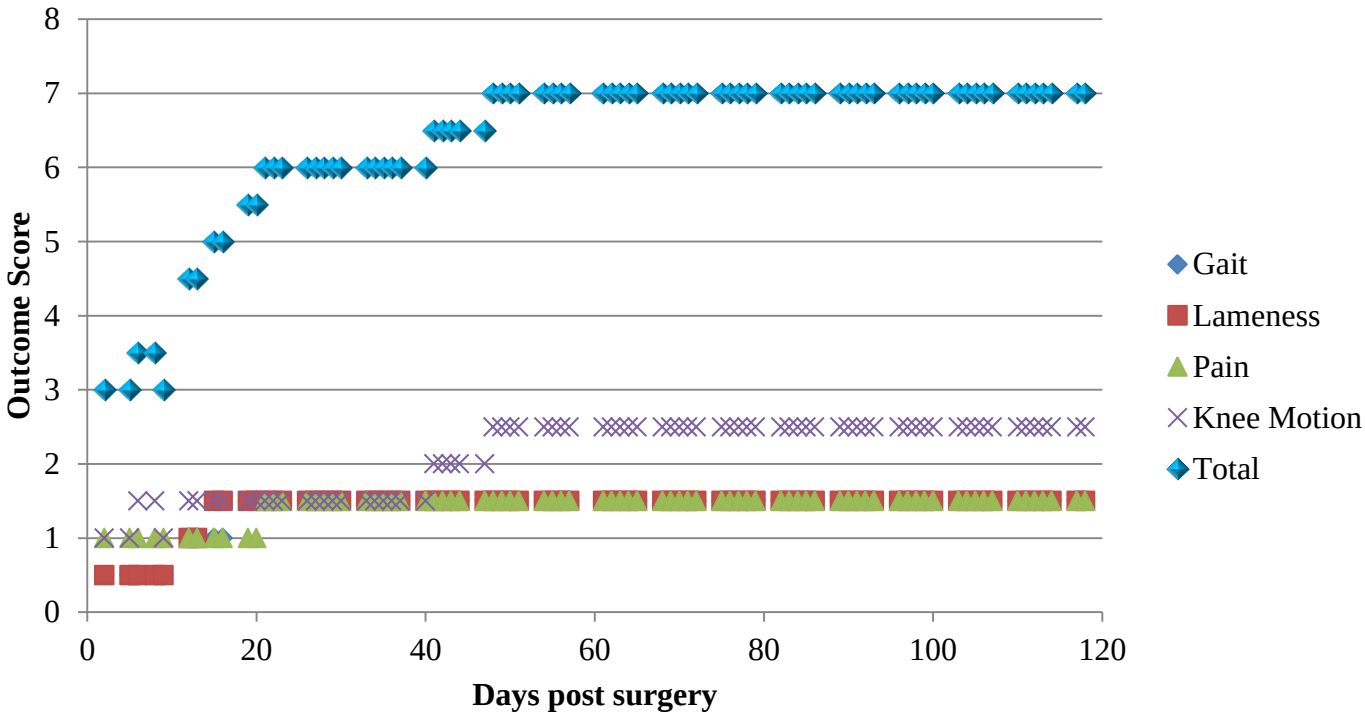

Figure 25: Outcome measurement for Segmental Defect Dog 18 (unseeded scaffold).

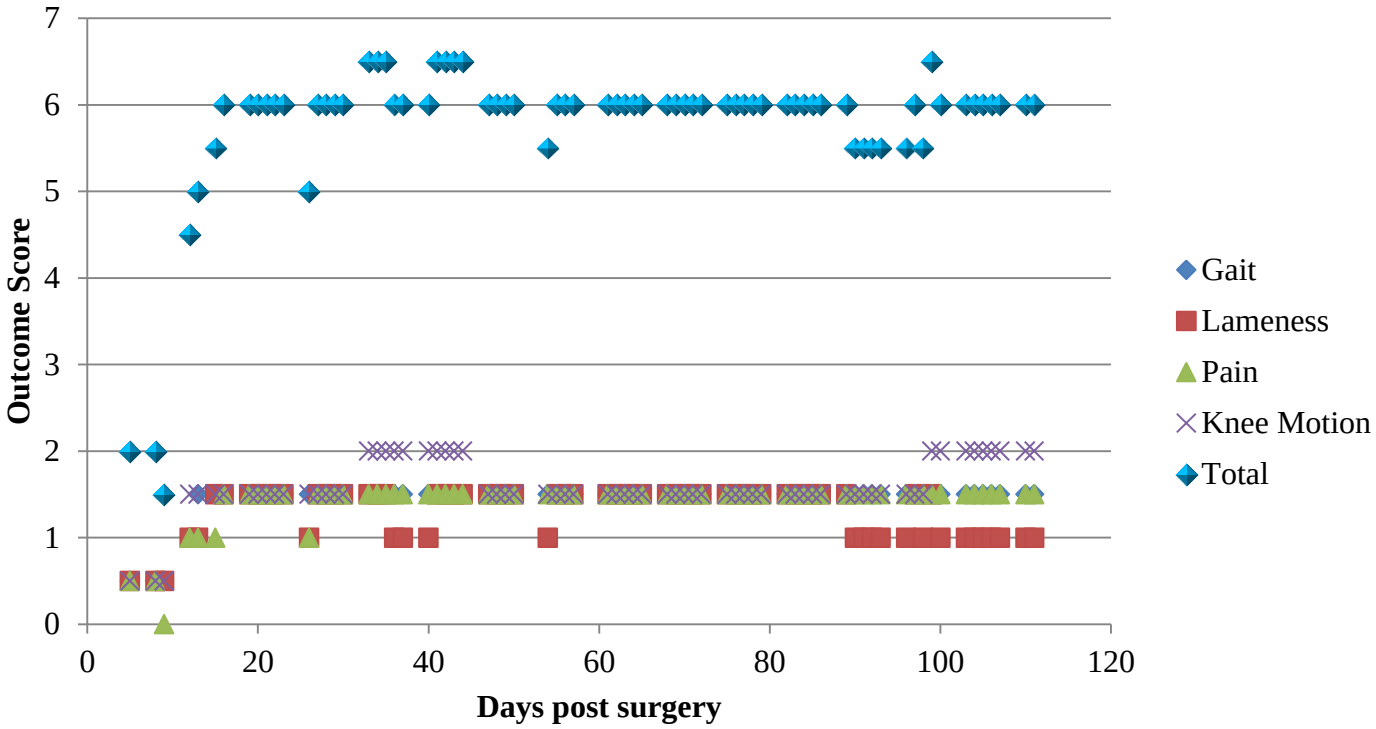

Figure 26: Outcome measurement for Segmental Defect Dog 19 (unseeded scaffold).

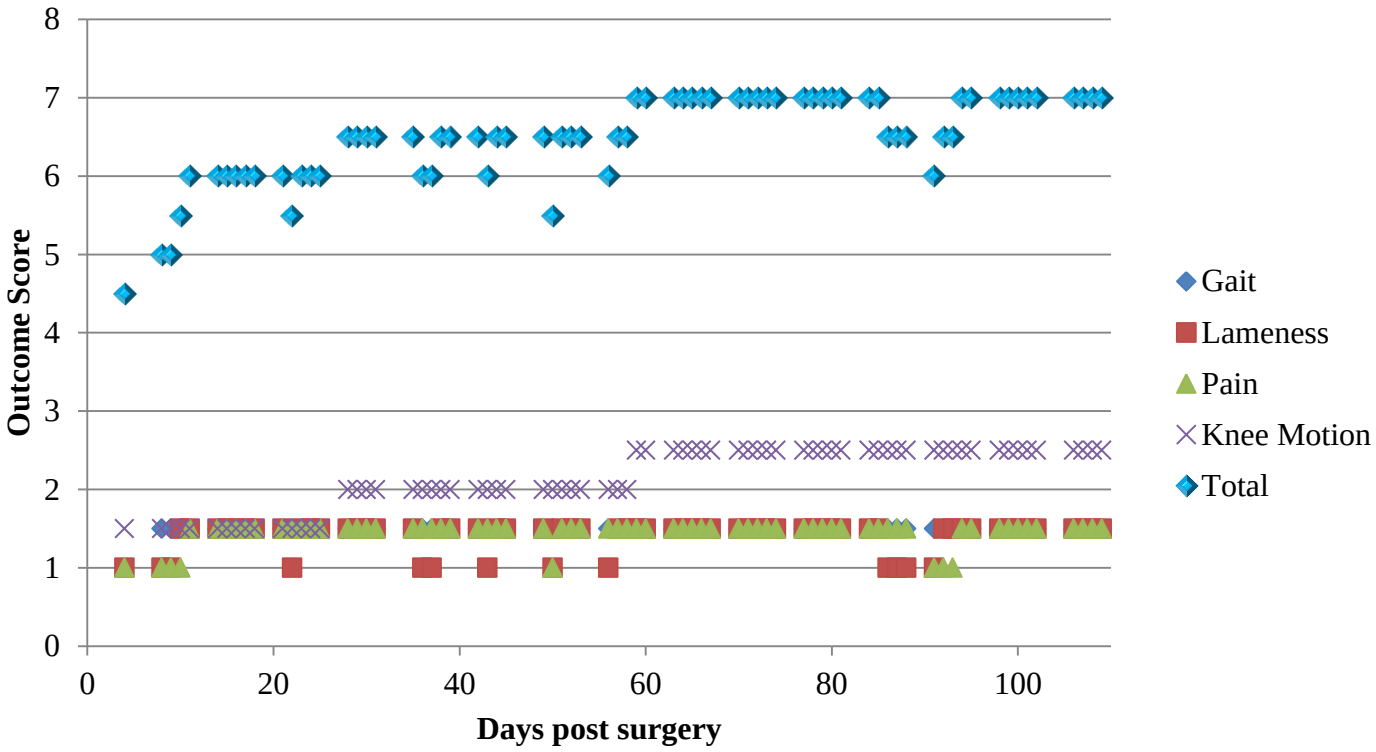

Figure 27: Outcome measurement for Segmental Defect Dog 20 (allograft).

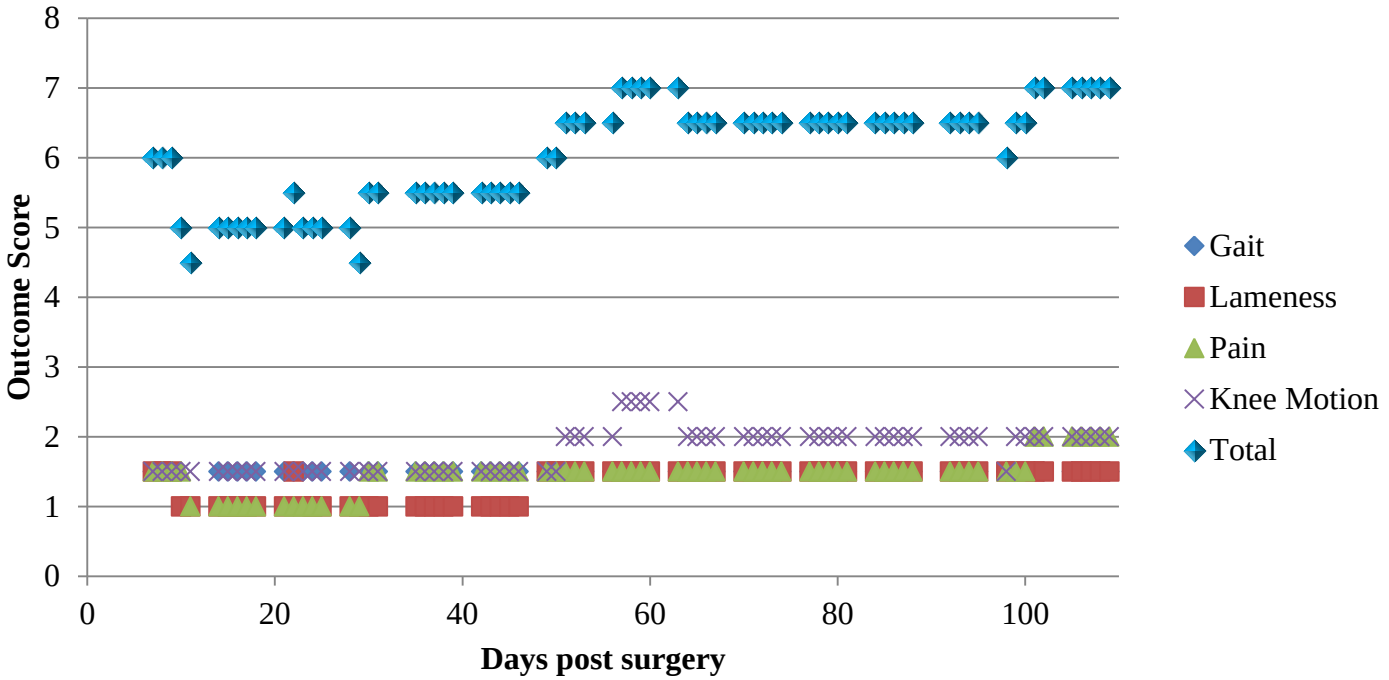

Figure 28: Outcome measurement for Segmental Defect Dog 21 (unseeded scaffold).

2.2.5 Segmental Defect Hard Sectioning Histology Study

Immediately following the mechanical testing, as reported in the 2013 Annual Report, the leg was removed from the testing jig and the resulting diaphyseal portion of the tested bone was then soaked in 10% formalin solution for over two months for fixation for future histological evaluation. Following fixation, the condyles underwent automatic dehydration and plastic infiltration (Leika TP 1020, Germany). The samples were put in a mold and covered with Technovit 7200 media (EXAKT, Germany). The submersed samples were than exposed to yellow and blue light Light Polymerization Utility (EXAKT, Germany) for a period of two days to create a hard specimen block. The specimen block was then trimmed with a band saw (EXAKT, Germany), and the cut surface was ground smooth with 800 or 1000 grit sandpaper. The smoothed side was then glued to a 4"× 2" plastic template slide by Technovit 7210 and the glue was hardened on a Light-Polymerization-Block-Sandwich machine (EXAKT, Germany) with blue light for 5 min. The process was repeated for the other side to create a specimen block sandwich. The block was then cut on a band saw with a 1 cm-wide diamond blade (EXAKT, Germany). The cut direction was parallel to the surface to be stained resulting in a 800~1000 μm thick slide specimen. To prepare the specimen for staining, the surface underwent a series of progressively finer polishings using 800 grit paper, 1000 grit paper and 1200 grit paper until only a 50~80 μm specimen layer was left. To eliminate scratches from cutting and grinding and to improve transparency of the slide surface, the specimen surface was polished with 4000 polish paper for more than one hour on the same grinding machine. The entire protocol followed the method provided by the EXAKT company(2). The slides were then stained with the standard Haematoxylin & Eosin (H&E) Stain or Masson's Trichrome Stain to distinguish connective tissues. The specimens for Dog 4 (shown in Figure 31 and 32) and Dog 5 (shown in Figure 29 and 30) were stained with both methods.

In all of the four histological slices (shown in Figure 29 ~ Figure 32), there were oblique gaps from the upper left to the bottom right that were spiral fractures caused by the torsional failure testing. Figure 29 and 30 are of the entire mid-diaphysis of right tibia implanted with a cadaveric allograft. The allograft is hard to distinguish due to its fusion with the tibial body. Figure 31(a) and 32(a) are of the entire mid-diaphysis of the right tibia, including the scaffold and associated callus. The scaffold regions can be distinguished by their appearance from the neighboring cortical bone. The bony ingrowth into most of the voids of the PCL-HA scaffold and the lumen, are shown in Figure 31(c) and 32(c). The bone covering of the scaffolds is mostly cancellous bone, which can be clearly identified from Figure 31(b) and 32(b), and cartilage, which as can be seen in the bottom parts of Figure 31(b) and 32(b). The black tissues through the entire tibia in the middle level represent the soft tissues of the bone marrow.

From the biomechanical test results previously reported in terms of failure torque and rotational energy, the failure torques of Dog 4 and Dog 5 were very close, possibly indicating a similar healing process for both allograft and unseeded scaffolds. The histological sections also show that the healing patterns on both kinds of implants were also very similar.

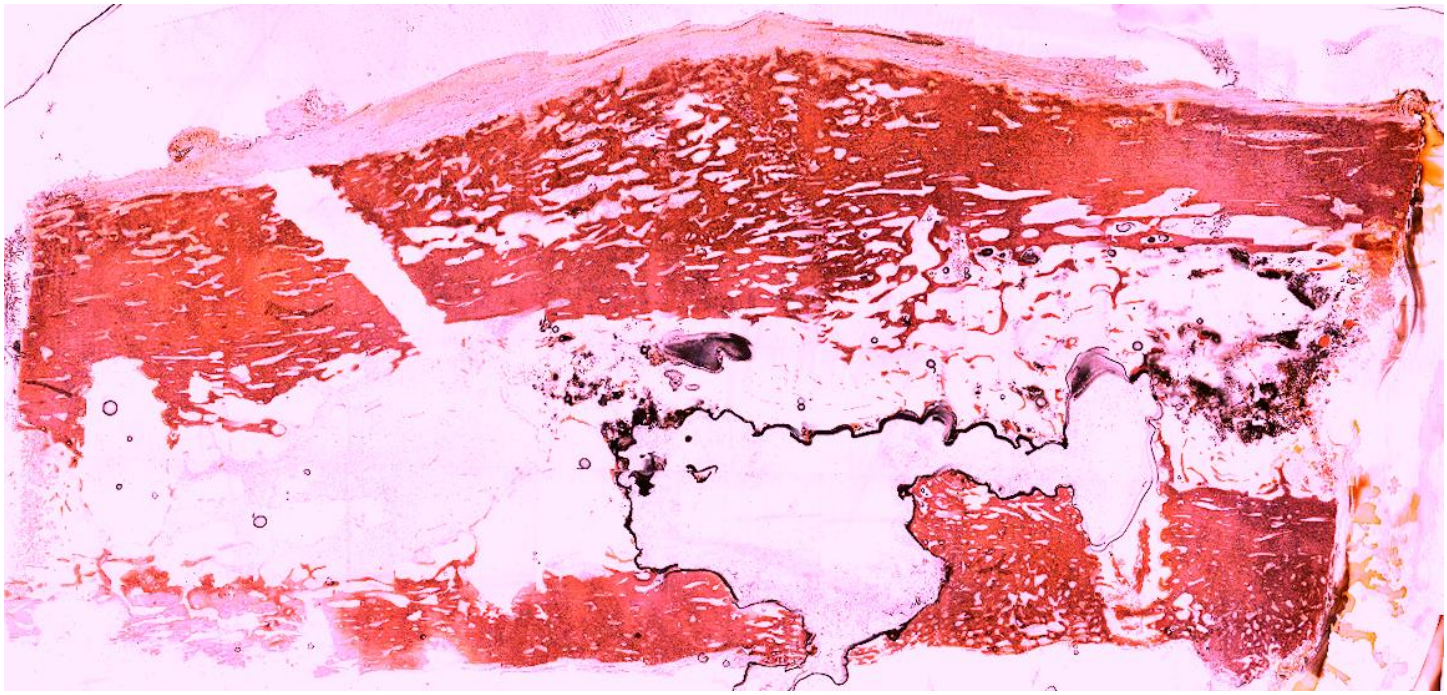

Figure 29: Hard sectioning histology image of Segmental Defect Dog 5 implanted with canine cadaveric allograft, stained by H&E method. Overview of mid-diaphysis of right tibia with canine cadaveric allograft. The oblique crack was the fracture generated by biomechanical testing.

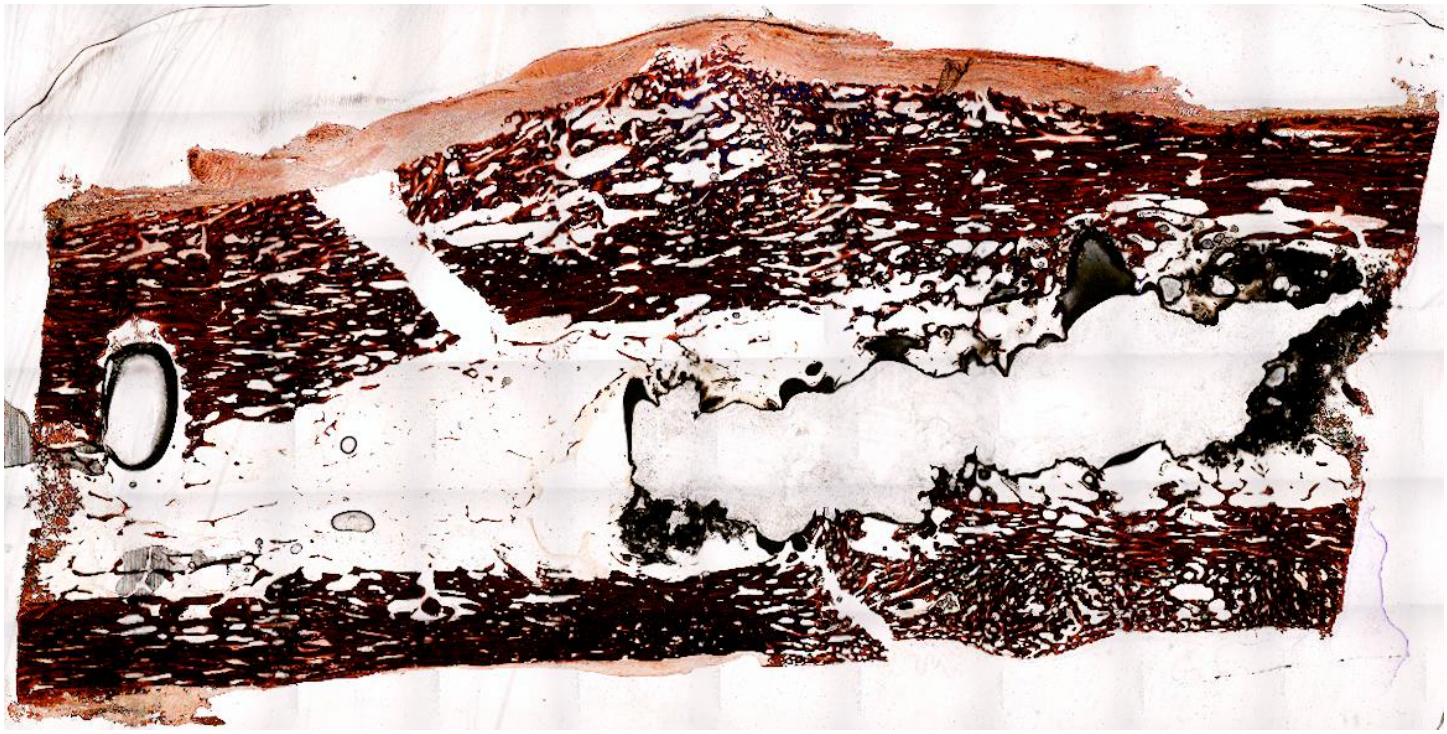

Figure 30: Hard sectioning histology image of Segmental Defect Dog 5 implanted with canine cadaveric allograft, stained by Masson's Trichrome method. Overview of mid-diaphysis of right tibia with canine cadaveric allograft. The black tissues in the middle level at right half are the bone marrow soft tissues. The oblique crack was the fracture generated by biomechanical testing.

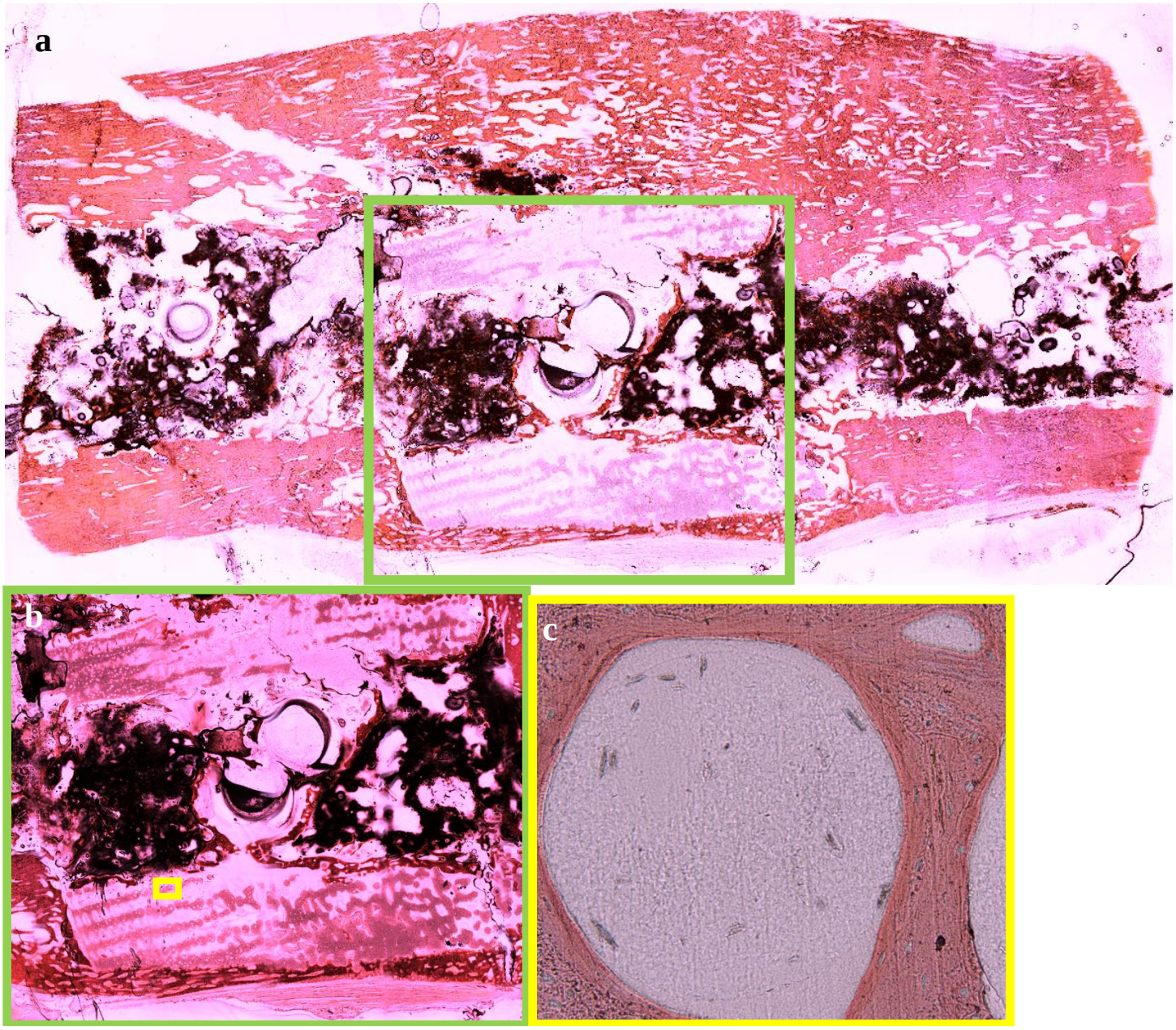

Figure 31: Hard sectioning histology image of Segmental Defect Dog 4 implanted with unseeded scaffold, stained by H&E method. (a) Overview of mid-diaphysis of right tibia with unseeded scaffold, (b) close-up of green rectangle region, (c) close-up of yellow rectangle region. The oblique crack was the fracture generated in biomechanical testing.

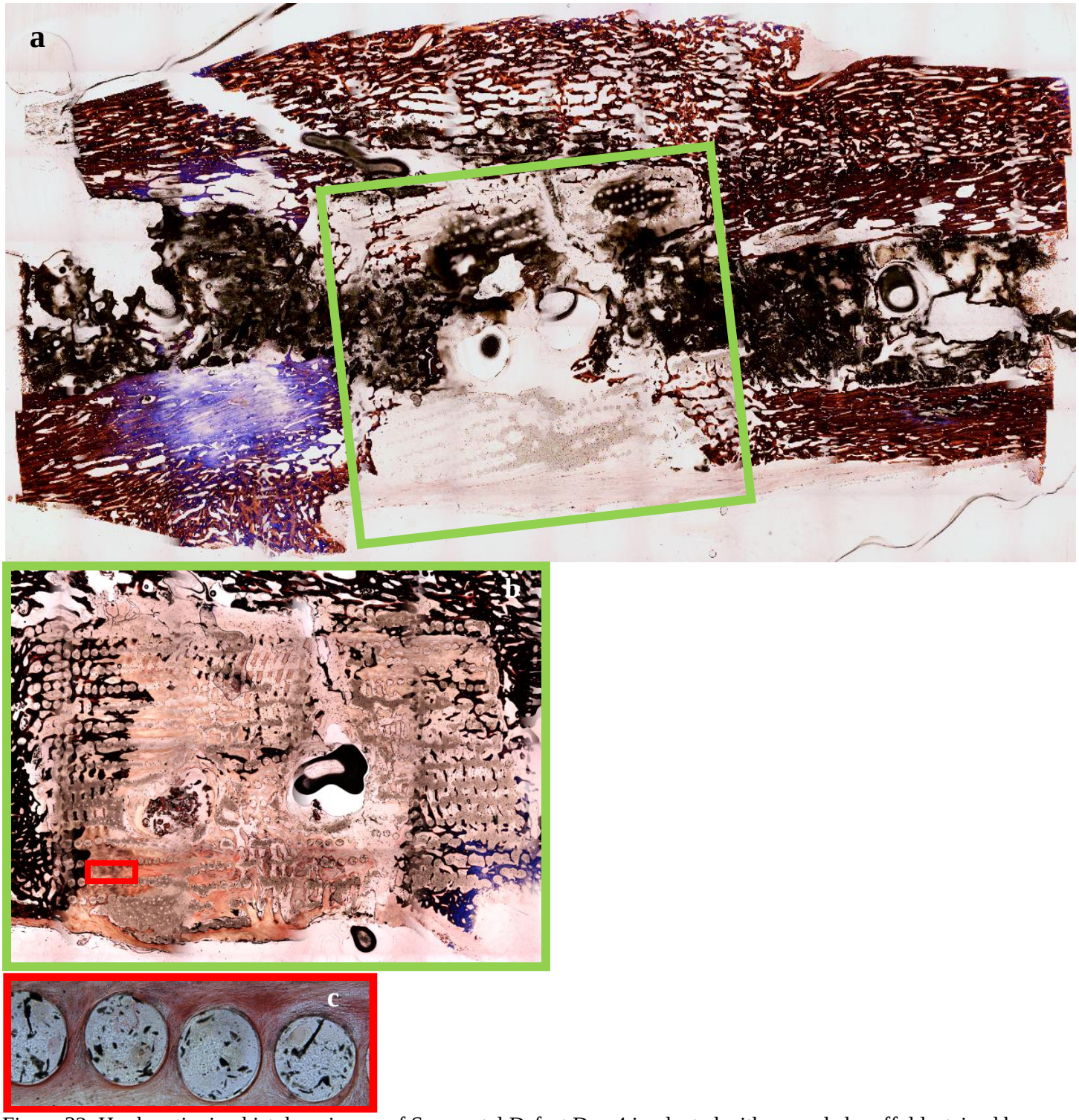

Figure 32: Hard sectioning histology image of Segmental Defect Dog 4 implanted with unseeded scaffold, stained by Masson's Trichrome method. (a) Overview of mid-diaphysis of right tibia with unseeded scaffold, (b) close-up of green rectangular region coming from another Trichrome-stained slice, (c) close-up of red rectangular region. The oblique crack was the fracture generated by biomechanical testing.

2.2.6 Study of BMP-2 Microspheres Attaching to the Surface of Scaffolds

BMP-2 microspheres were synthesized with BMP-2 protein encapsulated into poly(DL-lactic-*co*-glycolic acid) (PLGA) microspheres through a double-emulsion procedure previously used by the co-PI of this grant(3). The microsphere attaching procedure incorporated a specified amount of hydrophobic microsphere powder suspended in pure ethanol followed by immersing the entire scaffold into the ethanol loaded with the microspheres and mixing for 20 minutes. The liquid soaked scaffolds were then placed on glass, and sprayed with the ethanol plus microspheres suspension. The scaffolds were air dried, followed by gas sterilization. The scaffolds with BMP-2 microspheres had the same apparent strength and a similar physical appearance as the unseeded scaffolds.

A BMP-2 attached segmental defect scaffold and an unseeded scaffold were selected for scanning electron microscopic (SEM) imaging study. The scaffold was sliced and intersected to around 1 mm thickness pieces by a sterilized scalpel. A piece was then attached to a 10 mm diameter SEM specimen disk with a special carbon double-side glue, and the specimen disk was dried overnight in a vacuum desiccator. The SEM test was done on a Zeiss Supra 55 SEM machine under 15 kV acceleration electron voltage. The SEM images of an unseeded scaffold piece and a BMP-2 scaffold piece are shown in Figure 33 (a) and (b) separately. The surface of the unseeded scaffold had a smooth surface with pore sizes of a few microns. The surface of the BMP-2 scaffold shows the attached microspheres. Because the specimen slices were specifically selected from the inner section of the scaffold, their SEM images prove that the BMP-2 microspheres can successfully enter into the body of the scaffold and attach to the surface of the inside walls.

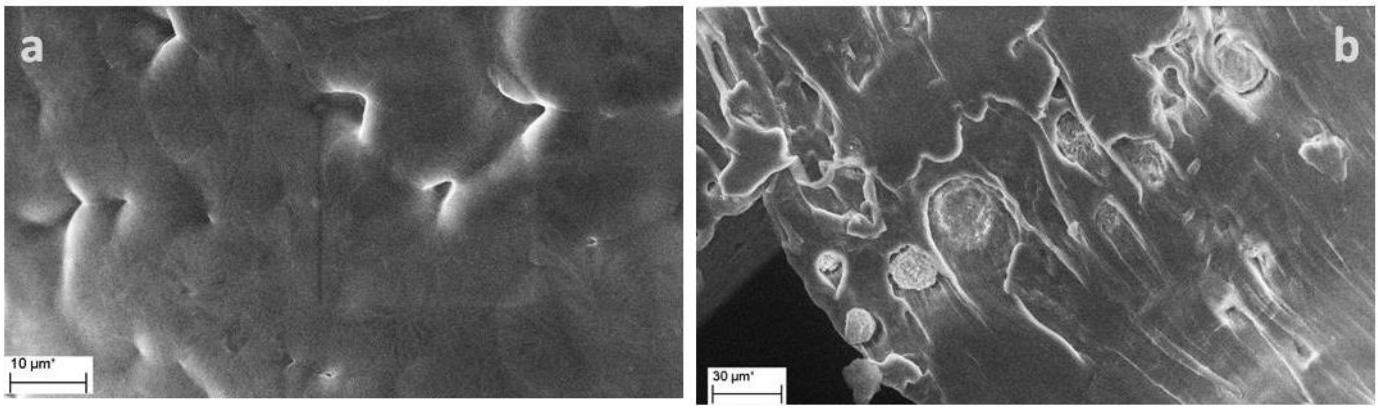

Figure 33: Scanning electron microscopic (SEM) image of the surface of the scaffolds in terms of (a) unseeded, and (b) seeded with BMP-2 microspheres.

2.2.7 *In-vitro* Study of Canine Stem Cell Expansion and Scaffold Seeding

Methodology

In accordance with our approved IACUC protocol, bone marrow aspirate was obtained in a sterile fashion from the segmental defect dogs immediately post-mortem. The bone marrow aspirate was obtained bilaterally from the iliac crest of the dog and immediately cultured.

BMSCs (Bone Marrow Derived Stem cells) derived from dog bone marrow were expanded in stem cell growth medium consisting of F12/DMEM (Life technologies Inc, MD, USA) supplemented with 20% (v/v) fetal bovine serum (Life technologies, USA) and 1% (w/v) Anti:Anti (Life technologies, USA). Osteogenic induction medium was prepared by adding 100 nM dexamethasone (Sigma) and 100 mg/ml L-ascorbic acid (Sigma) to the MEMa media) supplemented with 10% (v/v) fetal bovine serum (Life technologies, USA) and 1% (w/v) Penicillin:Steptomycin (Life technologies, USA). To induce osteogenic differentiation, BMSCs were seeded (10X5 cells/cm2) and cultured onto the PCL-HA scaffold in osteogenic induction medium with BMP-2 (50ng/ml) or without in 5% CO2 at 37°C. Cells were cultured in the stem cells growth medium for the first 10 days and in the osteogenic induction medium for the following days. We used BMBCs from Segmental Defect Dog 19 ~ 21 for the experiments.

Live-Dead Staining

Initial cell viability was examined by fluorescence cell viability assay based on the simultaneous determination of live and dead cells with two probes that measure recognized parameters of cell viability (LIVE-DEAD Cell Staining Kit, Cambridge, MA, USA). After 7 days from seeding on the scaffold, cells were washed three times with PBS. The supplied cell-permeable green fluorescent dye (Ex/Em = 488/518 nm) and propidium iodide (PI), a cell non-permeable red fluorescent dye (Ex/Em = 488/615) was diluted with PBS and the cells on the scaffold were dyed using the aqueous working solution for 30 min in 5% CO2 at 37°C. After washing three times with PBS, the cells on the scaffold were placed on the cover glass and the observation was performed using a fluorescence microscope (Axiovert 2000, Carl Zeiss, Germany). These fluorescence images were shown in Figure 34. We found only a few dead cells.

Measurement of Cell viability on PCL-HA scaffold

To evaluate cell viability, we made a standard curve using optical density (OD) from MTT assay (Roche Applied Science, Indianapolis, IN, USA). We measured the OD using MTT assay and we converted the OD to a cell number

relative to the standard curve. The BMSCs were used for cell viability assay. Four hundred µl of cell suspension was added to the scaffold at a density of 1 × 103 cells/scaffold. After 4 hours, 600 µl of growth medium was carefully added to the 12 wells plate. After culturing for 1 day in the plate, the cell/scaffold constructs were transferred to another 12 well plate, and 100 µl of media that included 50 µl of MTT reagent were added to each well and incubated at 37°C for 4 hours. An additional 500 ul of the solubilization solution was added to each well and incubated overnight. The absorbance at 570 nm was recorded using a Vermax microplate reader. The proliferation was evaluated after 7 days of culturing. The results shown in Figure 35 indicatethat the BMP positive group had higher cell numbers compared with the BMP negative group at day 7 and day 14.

Immunocytochemistry

The BMSCs were seeded onto the scaffold at a density of 1 × 106 cells. Twenty-four hours later, media was replaced with fresh media. At indicated times, cells were fixed with 4% formaldehyde and permeabilized with 0.1% Triton X in PBS buffer. Non-specific binding was reduced by incubation in 1% BSA in PBST (0.1% Tween-20) at room temperature for 1 hour. The scaffolds were incubated overnight at 4°C with primary antibodies against COL1A1 primary antibody (1:100; Santa Cruz, USA), washed in PBST, and incubated with AF568-labeled secondary antibody (1:200; Life Technologies, USA) for 1 hour at room temperature. Nuclear staining was achieved with VECTASHIELD with DAPI (Vector Laboratories Inc., USA). Actin staining was achieved with FITC-phalloidin (Life Technologies, USA). The immunocytochemical fluorescence images at the same time point were shown in Figure 36.

Quantification of Osteogenic markers

Scaffolds were washed with PBS and total RNA was collected using Trizol reagent (Life Technologies) according to the manufacturer's protocol. Total RNA (200 ng) was reverse-transcribed with Maxima First-Strand cDNA synthesis kit (Thermo Fisher Scientific Inc., USA). Real-time Quantitative PCR was performed with SYBR Select Master Mix UG (Life Technologies, USA) using QuantStudio 6 Flex (Life technologies, USA). Amplification conditions were 50°C for 2 min, 95°C for 10 min, followed by 40 cycles of denaturation (15 s at 95 °C), annealing (15 s at 60°C) and elongation (20 s at 72 °C). Quantitative PCR results were normalized to the loading control (Beta-actin) transcript level to yield ΔCt, then normalized to control conditions (e.g., normoxia at the same time point) to generate ΔΔCt. Relative or fold change in expression was subsequently calculated using the formula 2ΔCt or 2ΔΔCt, respectively. As shown from Figure 37, there was a higher osteogenic gene expression level in the BMP positive group than in the BMP negative group according to the MTT assay result and the qualification results from fluorescence images.

Summary

A variety of growth factors control stem cell to osteogenic differentiation. In an *in-vitro* experiment, we tested a recombinant human bone morphogenetic protein-2 (rhBMP-2) with the PCL-HA segmental defect scaffold to induce the differentiation of canine BMSCs towards osteogenic lineages, demonstrating the potential for scaffolds infused with canine BMSCs to promote bone infiltration and growth. Our approach was more efficient in the presence of rhBMP-2 rather than in the absence of rhBMP-2. The combined effects of biochemical signals from rhBMP-2 and scaffold stimulation on cell proliferation of canine BMSCs were examined in culture with and without soluble osteogenic factors (Figure 34 and 35). Furthermore, the rhBMP-2-added PCL-HA increased expression of RUNX2 and COL1A1 by the cells compared to those without BMP-2 (Figure 36 and 37). We conclude that the combination of BMP-2 and the scaffold stimulated cell proliferation and differentiation in the *in-vitro* study. The next steps will be the *in vivo* testing of this finding in the canine BMSC infused scaffold arm of Aim 2 (segmental defects) and the BMP2 + BMSC infused scaffold arm of Aim 2.

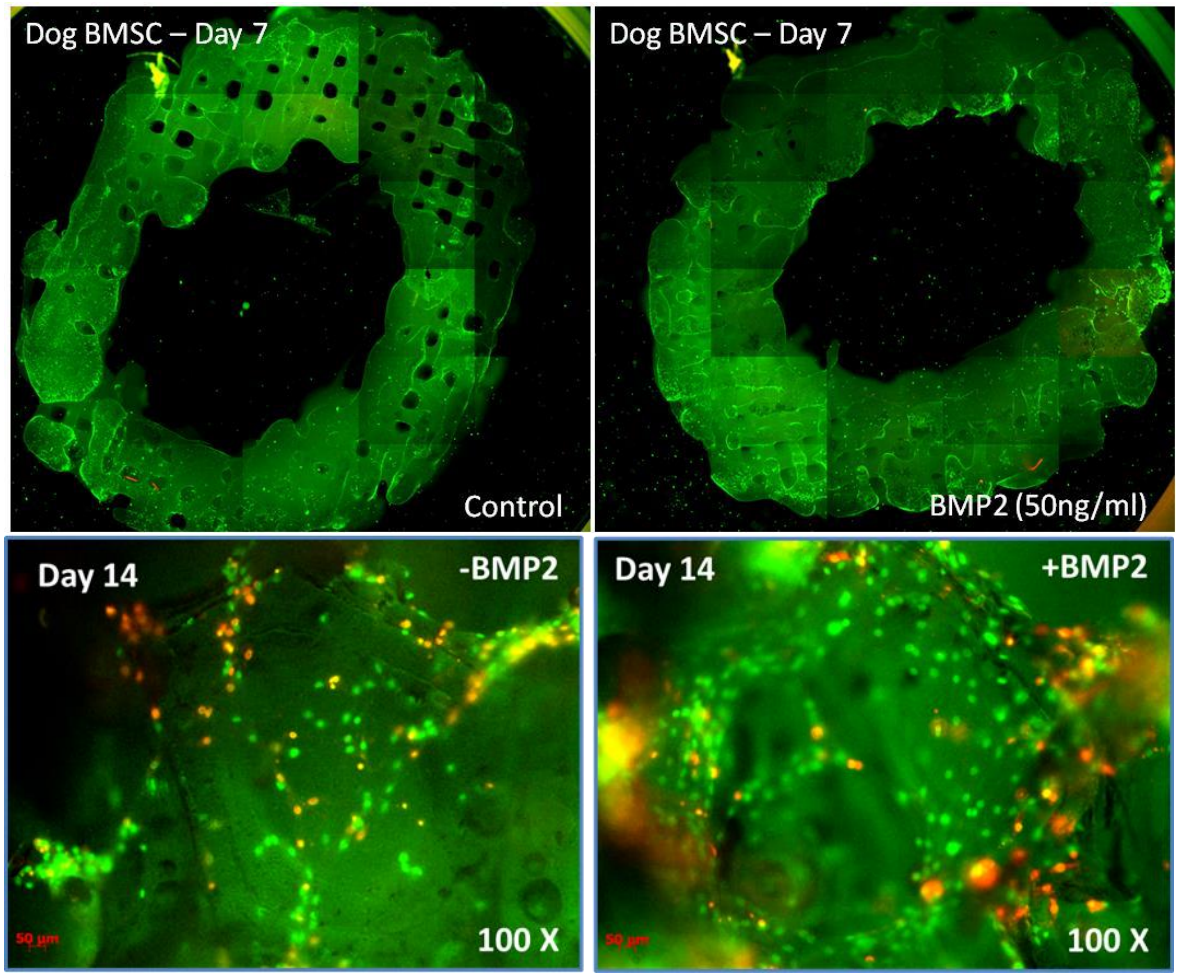

Figure 34: Live and dead assay of BMSCs on PCL-HA scaffold. Live cells were shown green and dead cells shown red. Most BMSCs were alive and gradually reached confluence at 14 days. Only a few cells were dead.

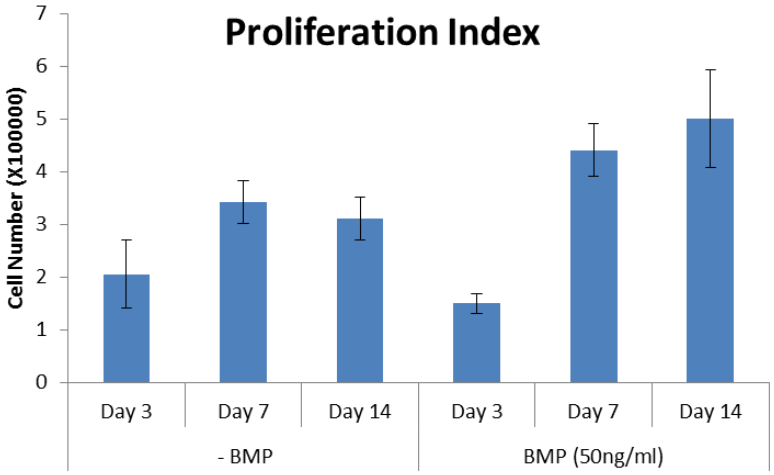

Figure 35: Quantification of viable cell number. There was significant difference between BMP with and without ($p < 0.05$).

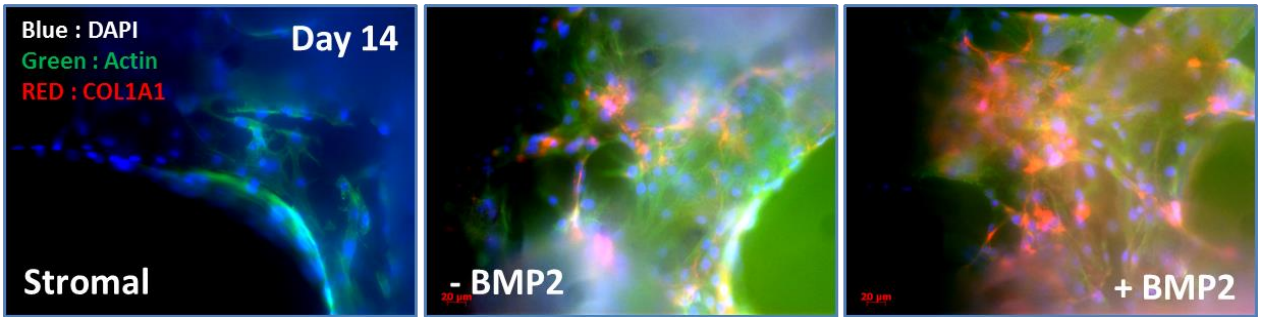

Figure 36: Fluorescence microscopic images of COL1A1 in BMSC cultured on PCL-HA scaffold for 14 days.

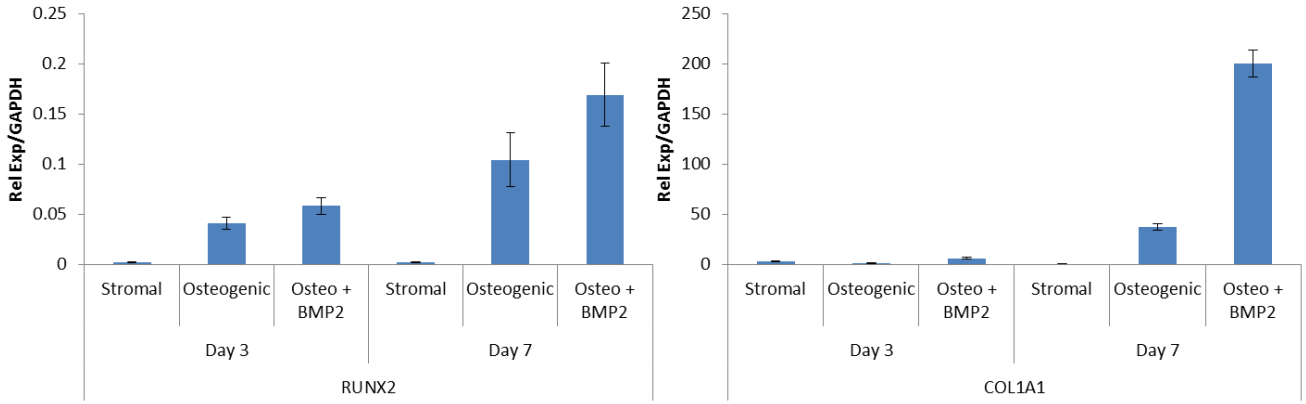

Figure 37: Related osteogenic gene expression levels in BMSC cultured on PCL-HA scaffold BMP2 with or without. Runx2 and Col1a1 gene expression levels were assessed by real-time PCR at days 3 and 7. GAPDH expression was also determined as an internal control. Significant differences between the groups are shown as ($p < 0.05$)

2.3 Aim 3 Human Cadaveric Testing

The results of the human cadaveric testing associated with the segmental defects reported in the 2013 Annual Report were written up in manuscript form and submitted to the Journal of Clinical Biomechanics in September 2014 and is attached as an appendix. We are awaiting the reviews.

3. KEY RESEARCH ACCOMPLISHMENTS

3.1 The PCL+HA mixture used to construct the scaffold was optimized on a new type of 3-D printer.

3.2 Eleven segmental defect surgeries (Aim 2) were performed and all successfully completed the full 16 weeks post-surgery recovery period without incident, supporting the use of the broad LCP plate.

3.3 There was no immune response by any of the animals to the slightly modified poly-caprolactone (PCL) and hydroxyapatite (HA) mixture and machine parameters used to manufacture the scaffolds with the new 3-D printer (Aim 2).

3.4 Outcome measures for segmental defect dogs (Aim 2) demonstrated that the surgical procedure was well-tolerated by the dogs and did not impair their quality of life.

3.5 Hard sectioning histology demonstrated tissue ingrowth in segmental defect dogs.

3.6 Scanning electron microscopy provided direct evidence that BMP-2 microspheres succeeded in attaching to the interior walls of the scaffolds.

3.7 All 8 surgeries using the unseeded scaffold experimental arm for Aim 2 (segmental defects) have been

completed.

3.8 The technique to obtain sterile bone marrow aspirate and culture canine stem cells was successfully demonstrated.

3.9 The combination of BMP-2 and the scaffold was shown to stimulate cell proliferations in an in-vitro study.

3.10 A manuscript based on the Aim 3 segmental defect human cadaveric testing results was submitted for review.

4. REPORTABLE OUTCOMES

A manuscript based on the results of our mechanical testing of human segmental defects reported in the 2013 Annual Report was submitted for review to the *Journal of Clinical Biomechanics*. The submitted manuscript is attached.

5. CONCLUSIONS

To date, 19 successful segmental defect surgeries have been completed and taken to the full 16 week recovery period (Aim 2). The use of a broad LCP plate successfully prevented adverse incidents. Hard histology was performed for the segmental defect dogs which showed connective tissue ingrowth into both unseeded scaffolds and allografts when adjacent to native bone. The outcome measures demonstrated consistent results between measurement metrics and clinical observations. They are felt to form a solid quantitative and qualitative approach to accurately assessing the results of surgical interventions. We have successfully demonstrated that canine stem cells can be cultured from bone marrow aspirate and will infiltrate the PCL-HA scaffold.

5.1 So What

Qualitatively, the addition of BMP-2 to the PCL-HA scaffolds seems to improve healing. However, this needs to be verified by mechanical testing. The successful expansion of canine stem cells from bone marrow aspirate and the infiltration of these cells into the PCL-HA scaffold will now allow us to proceed to the remaining two experimental arms of Aim 2, scaffolds seeded with canine stem cells and scaffolds seeded with BMP-2 plus canine stem cells.

6. REFERENCES

1. Lee CH, Cook JL, Mendelson A, Moioli EK, Yao H, Mao JJ. Regeneration of the articular surface of the rabbit synovial joint by cell homing: a proof of concept study. Lancet. 2010;376(9739):440-8. doi: 10.1016/S0140-6736(10)60668-X. PubMed PMID: 20692530.
2. Rohrer MD, Schubert CC. The cutting grinding technique for histologic preparation of undecalcified bone and bone-anchored implants. Oral Surg Oral Med Oral Pathol. 1992;74:73-8. Epub 78.
3. Moioli EK HL, Mao JJ. Inhibition of osteogenic differentiation of human mesenchymal stem cells. Wound Rep Reg. 2007;15:413-21.

7. APPENDICES

Manuscript submitted to *Journal of Clinical Biomechanics*, **"**Optimal Internal Fixation of Anatomically Shaped Synthetic Bone Grafts for Massive Segmental Defects of Long Bones", George C. Vorys, MD, Hanying Bai, Ph.D., Chandhanarat Chandhanayingyong, M.D., Chang H Lee, Ph.D.*, Jocelyn T. Compton, M.S., Jon-Michael Caldwell, M.D., Thomas R. Gardner, MCE, Jeremy J. Mao, DDS, PhD*, Francis Y. Lee, MD, PhD

Optimal Internal Fixation of Anatomically Shaped Synthetic Bone Grafts for Massive Segmental Defects of Long Bones

George C. Vorys, MD, Hanying Bai, Ph.D., Chandhanarat Chandhanayingyong, M.D., Chang H Lee, Ph.D.*, Jocelyn T. Compton, M.S., Jon-Michael Caldwell, M.D., Thomas R. Gardner, MCE, Jeremy J. Mao, DDS, PhD*, Francis Y. Lee, MD, PhD

Robert Carroll and Jane Chace Carroll Laboratories, Department of Orthopaedic Surgery, College of Physicians and Surgeons of Columbia University, New York, New York, U.S.A.

*Center for Craniofacial Regeneration, School of Dental Medicine, Columbia University, New York, New York, U.S.A.

Corresponding Author:

Francis Y. Lee, MD, PhD
Robert Carroll and Jane Chace Laboratories Professor
Professor of Orthopaedic Surgery
Department of Orthopaedic Surgery
E-mail: fl127@columbia.edu
Phone: (212) 305-7965

Abstract:

Background: Large segmental bone defects following tumor resection, high-energy civilian trauma, and military blast injuries do not heal well and present significant clinical challenges. Tissue engineering strategies which use scaffolds are being considered as a treatment of this clinical problem but there has been little research into optimal fixation of such scaffolds.

Methods: Twelve fresh-frozen paired cadaveric legs were utilized to simulate a critical sized intercalary defect in the tibia. Five cm anatomically correct poly-ε-caprolactone and hydroxyapatite composite scaffolds were fabricated, inserted into a tibial mid-diaphyseal intercalary defect and fixed with a 14-hole large fragment plate. Optimal screw fixation was tested by comparing non-locking and locking screws. Specimens were tested in axial, bending, and torsion in a non-destructive manner. A cyclic torsional test to failure under torque control was then performed.

Findings: Biomechanical testing showed no significant difference for bending or axial stiffness with non-locking vs locking fixation. Torsional stiffness was significantly higher ($p=0.002$) with the scaffold present for both non-locking and locking compared to the scaffold absent. In testing to failure angular rotation was greater for the non-locking compared to locking constructs at each torque level up to 40 N-m ($P < 0.05$). The locking constructs survived a significantly higher number of loading cycles before reaching clinical failure at 30 degrees of angular rotation ($P < 0.02$).

Interpretation: The presence of the scaffold increased the torsional stiffness of the construct. Locking fixation resulted in a stronger construct with increased cycles to failure compared to non-locking fixation.

1.0 Introduction

Massive skeletal defects of the tibia following high-energy civilian and military trauma or extensive resection of tumors remain a therapeutic challenge. Large bony defects occur in a small minority (0.4%) of fractures overall, but are common (11.4%) in open fractures.[1] In the tibia defects greater than 2 cm are unlikely to heal without additional bone grafting and defects greater than 5 to 6 cm are difficult to manage with autologous bone graft alone.[1-3] A number of surgical techniques exist to address these larger defects but require multiple procedures and significant morbidity with a high rate of complications.

Segmental allografts have been advocated to reconstruct defects after tumor resection and trauma but have a non-union rate as high as 17.3% and fracture rate of 17.7%.[4, 5] Distraction osteogenesis has been shown to be effective but also requires multiple procedures, an extended period of protected weight bearing with a bulky external fixator, and carries a re-fracture rate of 5% and amputation rate of 2.9%.[6] It also loses effectiveness for defects larger than 6 to 8 cm.[6, 7] Vascularized free fibula grafting is a viable option as well but requires specialized surgical skill as well as significant donor site morbidity.[8, 9] More recently a staged procedure with placement of a poly(methyl methacrylate) spacer to induce an osteogenic membrane followed by autogenous bone grafting has been advocated and shown to be effective for defects up to 20 cm.[2, 10, 11]

While effective, these techniques all require multiple procedures and carry significant donor site morbidity for bone grafting.[9] Tissue engineering has emerged as a promising approach for addressing large bony defects. The triad of tissue engineering has been proposed as a scaffold to provide structural stability as well as a platform for delivery of osteogenic growth factors and/or cells.[12] Scaffolds are now able to be designed with the correct micro and macro architecture for bony ingrowth and vascularization with promising results in animal studies.[13-17] The load-bearing capacity of the bone scaffold-fixation construct in human patients is an important factor in order to guide post-operative rehabilitation. However, most of previous studies focused on bone regeneration rather than the weight-bearing capacity of the bone scaffold-fixation construct.

Plate and screw fixation is commonly used for forearm bone fractures. For femur and tibia, intramedullary nailing is a common choice of internal fixation. For the humerus, both plate and screws and intramedullary nailing are used. However, for skeletal defects following resection of malignant tumors, intramedullary nailing is not conceptually preferred due to a theoretical concern of spreading tumors into the proximal and distal host bone and soft tissues during nail introduction and reaming.

In the present study, we examined the load-bearing capacity and optimal internal fixation of a bone/poly-ε-caprolactone-hydroxyapatite (PCL-HA) composite scaffold/plate construct that was anatomically fabricated in order to match the 5 cm segmental defect in the human tibia. We compared the non-locking versus the locking plate and screw constructs because one of the future indications for biocompatible and biomechanically competent scaffolds will be massive defects following tumor surgeries. Numerous biomechanical studies have demonstrated the mechanical superiority of locking fixation in a fracture model but none have focused on fixation of the bone scaffolds.[18-20] We hypothesized that the locking plate fixation provides more stable internal fixation under cyclic axial, bending, and torsional loading. The study is clinically relevant in that it will guide treating surgeons with respect to internal fixation and guide post-operative regimens for the patients with massive intercalary skeletal defects treated with bone scaffolds.

2.0 Materials and Methods

2.1 Fabrication of Intercalary Tibia Scaffolds

The anatomical morphology of a native cadaver adult human tibia was acquired from computed tomography scans on a clinical machine (SIMENS/Biograph 40, Malvern PA, USA) and manipulated using computer-aided design software for 3D modeling (Mimics, Materialise Co., USA). A 5 cm mid-shaft anatomically correct model of the tibia was designed. A composite polymer scaffold was fabricated using layer-by-layer deposition with a 3D printing system (Bioplotter, EnvisionTec, Berlin, Germany). The composite consisted of 90 wt% poly-ε-carpolactone (PCL) and 10 wt% hydroxyapatite (HA) (Sigma, St. Louis, MO, USA). PCL-HA composite was molten in the chamber at 120°C and dispensed through an 18 Ga needle to create interlaid strands and interconnected micro-channels (diameter 400 μm). We selected this PCL-HA composite in accordance with previous findings of cell adhesion and osteochondral histogenesis using the same material.[14]

2.2 Implantation of Structural Scaffolds into the Intercalary Defect of the Tibia

Twelve fresh-frozen cadaveric limbs from six individuals (6 pairs, average age 75, range 72 – 78, 4 males, 2 females) were utilized in this study. An antero-lateral incision was made and the lateral aspect of the tibia was exposed sharply. The surrounding soft tissue and fibula were maintained and a 5 cm section of tibia removed from the diaphysis. A 14-hole 4.5 mm broad, 260 mm large fragment locking compression plate from Synthes (Paoli, PA) was placed provisionally with bone clamps. The scaffold was provisionally placed with suture augment around the plate. The plate was fixed with five 5.0 mm diameter locking screws superior and inferior to the scaffold. Two 4.5 mm diameter cortical screws were placed into the scaffold to secure it. All screws bridged both cortices. The plate was contoured slightly at the distal end to conform to the distal tibia surface. All soft tissue was removed for biomechanical testing.

2.3 Biomechanical Testing

The tibial plateau was cut to create a square end that was placed within a square fiberglass tube. Orthogonal Steadman pins were passed through the tube and bone and the entire construct filled with poly(methyl methacrylate). A metal plate with a spherical depression and a steel ball was placed on top of the fiberglass tube when axial compression was applied and the tibia was loaded via a flat platen. When torsion loading was applied, the plate and ball were removed and square clamp was lowered around the fiberglass tube that allowed for axial motion while preventing any slippage in rotation. The distal end of the tibia was potted in the same manner as the proximal end and placed within a square clamp rigidly connected to the biaxial load cell. Torsional loading was applied at the proximal end of the tibia. (Fig. 1)

Loading was applied with a MTS 858 Bionix (MTS Eden Prairie, MN, USA) testing system. Axial loading was applied via a series of step loads of 50 N, 400 N, 500 N, 600 N and 700 N. At each step, the load was applied in a sinusoidal fashion for 50 cycles at a rate of 2 Hz. Data were collected at a rate of 10 Hz. Three-point bending loads were applied to the middle of the plate also via a series of step loads of 50 N, 200 N, 250 N, 300 N and 350 N in the same manner as was done for the axial loading. Bending supports were placed 27.9 cm apart for all specimens. Mid-span displacements were recorded with a MTS Model 632.03 extensometer. Finally, a sequence of increasing sinusoidal torsional moments of ±3, ±6 and ±9 N-m were applied for 20 sinusoidal cycles at a rate of 0.5 Hz. The loading sequence was randomized for each pair, but was the same for each leg of a pair. Following sub-failure testing with the scaffold in place, the scaffold was removed and the same series of tests repeated without the scaffold. The order of scaffold / no scaffold was not randomized because the main intent of the study was to determine the stiffness of the construct with the scaffold in place. Specimens were then loaded to failure in torsion with the scaffold absent. A sequence of increasing sinusoidal torsional moments of ±10, ±15, ±20, ±25, ±30, ±35, ±40, and ±45 N-m were applied at 0.5 Hz for 25 cycles at each level of torsional loading and allowed to continue indefinitely at the ±45 N-m level until failure.

2.4 Statistical Analysis

Separate statistical analyses were performed for the non-destructive and failure testing. Two-way repeated measures ANOVAs (SAS, Cary, NC) were performed for non-destructive testing. Factors were fixation type (locking, non-locking screws) and scaffold condition (scaffold present, scaffold absent). Axial stiffness, bending stiffness and torsional stiffness were the measured parameters. Two-way repeated measures were also performed for failure testing with the factors of fixation type (locking, non-locking screws) and torsional load (±10, ±15, ±20, ±25, ±30, ±35, ±40, and ±45 N-m). Student-Newman Keuls multiple comparisons tests were used to discern differences between loading levels. Statistical significance was taken as $P < 0.05$.

3.0 Results

3.1 Non-Destructive Testing

There was no significant difference in axial stiffness, bending stiffness for locking vs. non-locking constructs both with and without the scaffold (Figs 2 and 3). For torsional stiffness there was no difference for locking vs. non-locking constructs but constructs with the scaffold present were significantly stiffer ($P < 0.002$, Fig 3).

3.2 Failure Testing

Specimens tended to gradually loosen as indicated by increasing angular rotation at each increasing torsional moment. The non-locking constructs demonstrated increased angular displacement at each step torque ($P < 0.05$, Fig 4) compared

to the locking constructs. It was appreciated that by 30 degrees of angular displacement specimens were grossly loose though still intact. We defined this amount of angular displacement as "clinical failure", i.e. the point at which constructs had irreversibly started loosening. Comparing the number of cycles to clinical failure, 30 degrees of angular displacement, between locking and non-locking constructs showed the locking constructs lasted an average of 203 cycles vs 66 cycles for the non-locking constructs ($P < 0.02$, Fig 5). At physical failure, the non-locking constructs tended to fail by screw loosening and gradual leveraging open of the bone whereas the locking constructs tended to fail with little widening of the crack along the screw line until the bone suddenly failed catastrophically (Fig 6).

4.0 Discussion

Massive segmental bony defects of the tibia remain very challenging to treat with a high percentage of patients experiencing complications of infection, non-union, fracture, and amputation. Tissue engineering strategies may provide improved implants for providing temporary stability as well as delivery of osteogenic growth factors and cells to promote bony healing.

A number of studies have looked at many different materials for bony scaffolds with a wide range of material properties.[21, 22] Some are very soft such as alginate gels or collagen sponges, intermediate such as PGA/PLA polymers and others are hard but brittle such as bioactive glasses and calcium triphosphate. PCL-HA demonstrates advantageous material properties, biocompatibility, and the ability to bind and deliver growth factors and cells as shown by previous work.[13, 14] This study showed that in either a locking or non-locking construct the presence of a PCL-HA scaffold has the ability to provide extra rigidity in torsion. Studies looking at bony incorporation of metal implants in arthroplasty have shown that too much motion at the interface can lead to fibrous tissue formation where more rigid constructs result in bony ingrowth. It may be the same in a bone-scaffold interface situation in fracture repair as well.

Our failure tests demonstrate significantly greater cycles to clinical failure for locking plate fixation compared to non-locking. No matter what strategy is used, large segmental bony defects are very slow to heal putting tremendous stress on fixation constructs. Use of locking fixation with a scaffold proved to be a more robust construct with increased resistance to failure than non-locking in this biomechanical study. Current treatments used in the treatment of bony defects are now most commonly an induced membrane followed by bone grafting or bone transport with distraction osteogenesis. With the induced membrane technique, regardless of whether the tibia is fixed with an IM nail or external fixator, an extended period of non-weight bearing is required, as the bone graft has no real mechanical stability when first implanted. Distraction osteogenesis requires an extended use of bulky external fixators as well as requiring that the patient remain non-weight bearing. Use of a PCL-HA scaffold and locking plates produce a rigid construct, which may allow earlier mobilization and partial weight bearing while treating large bone defects. A locking plate also has the theoretical advantage of less disruption of the fracture healing biology because the plate is not tightly compressed against the bone as with a non-locking construct.

There are several limitations to this study. This is an in-vitro lab biomechanics study and therefore only able to assess the stability of the construct at time zero. *In vivo*, the biomechanics of healing fractures and fixation constructs change dynamically as the bone heals, forms callous, and remodels. This model also represents a best-case scenario where the bone defect was placed in the middle of the diaphysis with clean cuts. It was also assumed when performing the statistical analyses that the left and right legs of an individual represented a repeated measures condition, i.e. it was assumed that there were no differences between left and right legs. The average age of 75 of the specimens is also much older than that of actual patients, though it is thought that this factor would not have a significant impact on the findings. Significant work remains to elucidate what is the ideal scaffold to use for bone tissue engineering applications and which growth factors or cellular augmentation should be employed. This study only sought to examine what fixation strategy would be best, independent of those issues. Future studies are needed in large animal models testing the feasibility and *in vivo* stability of scaffold-based repair of large bony defects.

5.0 Conclusions

Tissue engineering with anatomically correct scaffolds presents an exciting new strategy for the treatment of critical size defects of the tibia. The presence of the scaffold was found to increase the torsional stiffness of the construct. Locking fixation resulted in a stronger construct with increased cycles to failure compared to non-locking fixation. It is envisioned that currently available locking plate-screw scaffold constructs may provide rigid enough fixation to allow early mobilization and weight bearing of patients with critical sized intercalary bone defects.

6.0 Acknowledgements

This study was supported by the U.S. Department of Defense contract number W81XWH-10-1-0933, grant number OR090175. Francis Y. Lee PI, Jeremy J. Mao co-PI and NIH grants AR065023 and EB009663, Jeremy J. Mao PI.

References

[1] J. Keating, A. Simpson, C. Robinson, J Bone Joint Surg Br., 87 (2005) 142-150.
[2] O. Aho, P. Lehenkari, J. Ristiniemi, S. Lehtonen, J. Risteli, H.-V. Leskelä, J Bone Joint Surg Am., 95 (2013) 597-604.
[3] J. May, J. Jupiter, A. Weiland, H. Byrd, J Bone Joint Surg Am., 71 (1989) 1442-1428.
[4] F. Hornicek, M. Gebhardt, W. Tomford, J. Sorger, M. Zavatta, J. Menzner, H. Mankin, Clin Orthop Relat Res., 382 (2001) 87-98.
[5] J. Sorger, F. Hornicek, M. Zavatta, J. Menzner, M. Gebhardt, W. Tomford, H. Mankin, Clin Orthop Relat Res., 382 (2001) 66-74.
[6] C. Papakostidis, M. Bhandari, P. Giannoudis, Bone Joint J., 95-B (2013) 1673–1680.
[7] S. Rigal, P. Merloz, N.D. Le, H. Mathevon, a.-C. Masquelet, Orthop Traumatol Surg Res., 98 (2012) 103-108.
[8] C. Han, M. Wood, A. Bishop, W. Cooney, J Bone Joint Surg Am., 74 (1992) 1441-1449.
[9] C. Myeroff, M. Archdeacon, J Bone Joint Surg Am., 93 (2011) 2227-2236.
[10] C. Karger, T. Kishi, L. Schneider, F. Fitoussi, a.-C. Masquelet, Orthop Traumatol Surg Res., 98 (2012) 97-102.
[11] B. Taylor, B. French, T. Fowler, J. Russell, A. Poka, J Am Acad Orthop Surg., 20 (2012) 142-150.
[12] H. Nie, C. Lee, J. Tan, C. Lu, A. Mendelson, M. Chen, M. Embree, K. Kong, B. Shah, S. Wang, S. Cho, J. Mao, Cell Tissue Res., 347 (2012) 665-676.
[13] C. Lee, J. Cook, A. Mendelson, E. Moioli, H. Yao, J. Mao, Lancet, 376 (2010) 440-448.
[14] C. Lee, N. Marion, S. Hollister, J. Mao, Tissue Eng Part A., 15 (2009) 3923-3930.
[15] A. Alhadlaq, J. Mao, J Bone Joint Surg Am., 87 (2005) 936-944.
[16] M. Oest, K. Dupont, H.-J. Kong, D. Mooney, R. Guldberg, J Orthop Res. , 25 (2007) 941-950.
[17] L. Amorosa, C. Lee, a.B. Aydemir, S. Nizami, A. Hsu, N. Patel, T. Gardner, A. Navalgund, D. Kim, S. Park, J. Mao, F. Lee, Int J Nanomedicine., 8 (2013) 1637-1643.
[18] E. Fulkerson, K. Egol, E. Kubiak, F. Liporace, F. Kummer, K. Koval, J Trauma., 60 (2006) 830-835.
[19] C. Davis, A. Stall, E. Knutsen, J Orthop Trauma., 26 (2012) 216-221.
[20] R. Will, R. Englund, J. Lubahn, T. Cooney, Arch Orthop Trauma Surg., 131 (2011) 841-847.
[21] A. Shrivats, M. McDermott, J. Hollinger, Drug Discov Today., 00 (2014).
[22] M. Mravic, B. Péault, A. James, Biomed Res Int. , (2014) 865270.

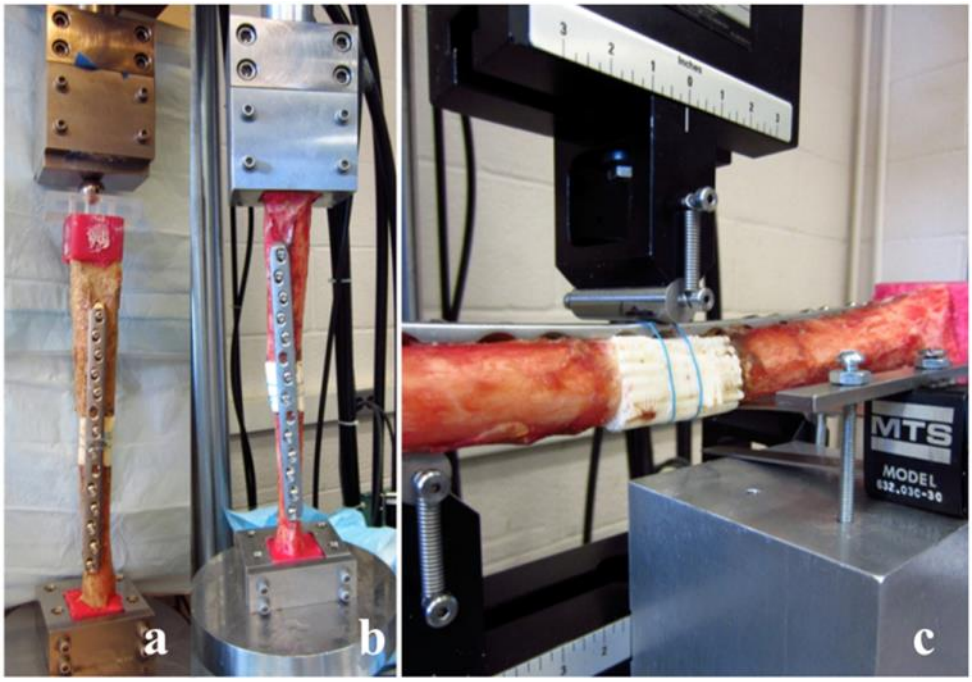

Figure 1. Mechanical testing of human cadaveric tibia with scaffold in segmental defect, (a) axial loading via ball bearing, (b) torsional loading via square clamp allowing axial displacement, (c) three-point bending of tibia-plate-scaffold construct, bending load is applied to the middle of the locking plate.

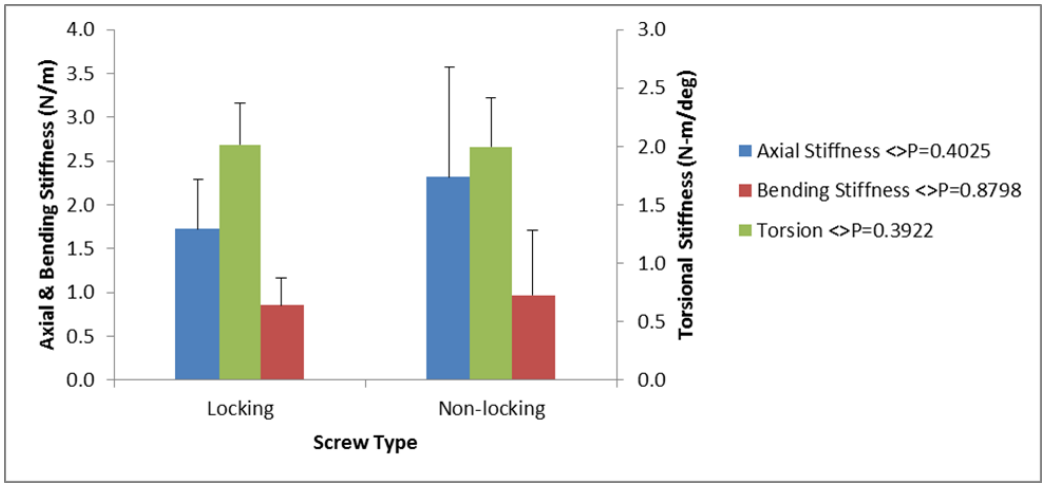

Figure 2. Axial, bending, and torsional stiffness for locking vs non-locking constructs. Error bars denote 1 standard deviation.

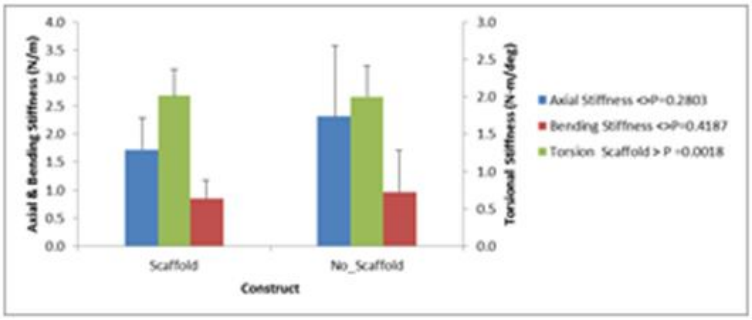

Figure 3. Axial, bending, and torsional stiffness for with and without scaffold. Error bars denote 1 standard deviation.

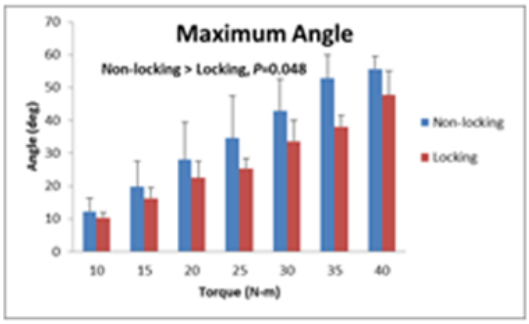

Figure 4. Maximum angular displacements as a function of torque for non-locking and locking constructs. Error bars denote 1 standard deviation.

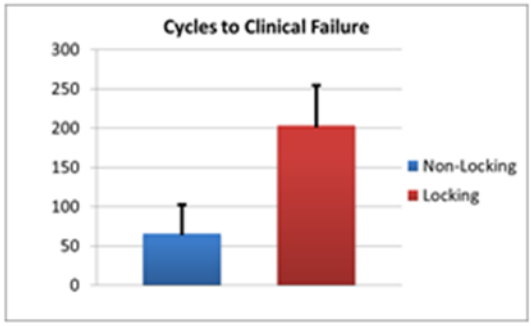

Figure 5. Cycles to clinical failure for non-locking and locking constructs. Error bars denote 1 standard deviation.

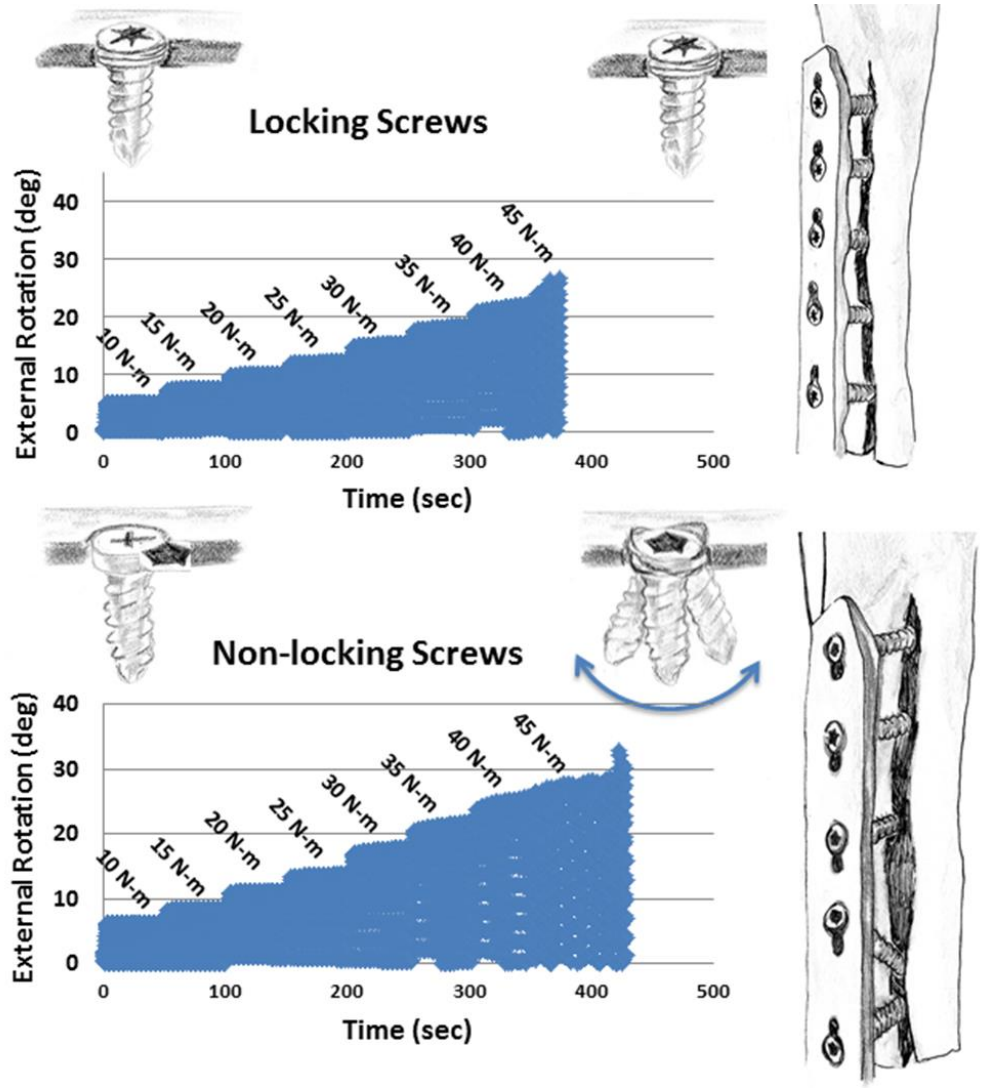

Figure 6. Depiction of locking screws and non-locking screws showing mechanism of loosening and crack formation. Note the the screw loosening, toggling and back-out for non-locking screw as compared to the locking screw that results in progressive widening of the crack. Plots are of representative failure tests showing tibial rotation as a function of time and applied torque for a paired specimen. Note the larger rotation at higher applied torques for the non-locking screw.